



# TECH BRIEFS

NATIONAL AERONAUTICS AND SPACE ADMINISTRATION

-  **Technology Focus**
-  **Computers/Electronics**
-  **Software**
-  **Materials**
-  **Mechanics**
-  **Machinery/Automation**
-  **Manufacturing**
-  **Bio-Medical**
-  **Physical Sciences**
-  **Information Sciences**
-  **Books and Reports**



## INTRODUCTION

Tech Briefs are short announcements of innovations originating from research and development activities of the National Aeronautics and Space Administration. They emphasize information considered likely to be transferable across industrial, regional, or disciplinary lines and are issued to encourage commercial application.

### Availability of NASA Tech Briefs and TSPs

Requests for individual Tech Briefs or for Technical Support Packages (TSPs) announced herein should be addressed to

#### National Technology Transfer Center

Telephone No. (800) 678-6882 or via World Wide Web at [www2.nttc.edu/leads/](http://www2.nttc.edu/leads/)

Please reference the control numbers appearing at the end of each Tech Brief. Information on NASA's Innovative Partnerships Program (IPP), its documents, and services is also available at the same facility or on the World Wide Web at <http://ipp.nasa.gov>.

Innovative Partnerships Offices are located at NASA field centers to provide technology-transfer access to industrial users. Inquiries can be made by contacting NASA field centers and Mission Directorates listed below.

## NASA Field Centers and Program Offices

#### Ames Research Center

Lisa L. Lockyer  
(650) 604-1754  
[lisa.l.lockyer@nasa.gov](mailto:lisa.l.lockyer@nasa.gov)

#### Dryden Flight Research Center

Gregory Poteat  
(661) 276-3872  
[greg.poteat@dfrc.nasa.gov](mailto:greg.poteat@dfrc.nasa.gov)

#### Goddard Space Flight Center

Nona Cheeks  
(301) 286-5810  
[Nona.K.Cheeks.1@nasa.gov](mailto:Nona.K.Cheeks.1@nasa.gov)

#### Jet Propulsion Laboratory

Ken Wolfenbarger  
(818) 354-3821  
[james.k.wolfenbarger@jpl.nasa.gov](mailto:james.k.wolfenbarger@jpl.nasa.gov)

#### Johnson Space Center

Helen Lane  
(713) 483-7165  
[helen.w.lane@nasa.gov](mailto:helen.w.lane@nasa.gov)

#### Kennedy Space Center

Jim Aliberti  
(321) 867-6224  
[Jim.Aliberti-1@nasa.gov](mailto:Jim.Aliberti-1@nasa.gov)

#### Langley Research Center

Ray P. Turcotte  
(757) 864-8881  
[r.p.turcotte@larc.nasa.gov](mailto:r.p.turcotte@larc.nasa.gov)

#### John H. Glenn Research Center at Lewis Field

Robert Lawrence  
(216) 433-2921  
[robert.f.lawrence@nasa.gov](mailto:robert.f.lawrence@nasa.gov)

#### Marshall Space Flight Center

Vernotto McMillan  
(256) 544-2615  
[vernotto.mcmillan@msfc.nasa.gov](mailto:vernotto.mcmillan@msfc.nasa.gov)

#### Stennis Space Center

John Bailey  
(228) 688-1660  
[john.w.bailey@nasa.gov](mailto:john.w.bailey@nasa.gov)

#### NASA Mission Directorates

At NASA Headquarters there are four Mission Directorates under which there are seven major program offices that develop and oversee technology projects of potential interest to industry:

##### Carl Ray

Small Business Innovation Research Program (SBIR) & Small Business Technology Transfer Program (STTR)  
(202) 358-4652  
[carl.g.ray@nasa.gov](mailto:carl.g.ray@nasa.gov)

##### Frank Schowengerdt

Innovative Partnerships Program (Code TD)  
(202) 358-2560  
[fschowen@hq.nasa.gov](mailto:fschowen@hq.nasa.gov)

##### John Mankins

Exploration Systems Research and Technology Division  
(202) 358-4659  
[john.c.mankins@nasa.gov](mailto:john.c.mankins@nasa.gov)

##### Terry Hertz

Aeronautics and Space Mission Directorate  
(202) 358-4636  
[thertz@mail.hq.nasa.gov](mailto:thertz@mail.hq.nasa.gov)

##### Glen Mucklow

Mission and Systems Management Division (SMD)  
(202) 358-2235  
[gmucklow@mail.hq.nasa.gov](mailto:gmucklow@mail.hq.nasa.gov)

##### Granville Paules

Mission and Systems Management Division (SMD)  
(202) 358-0706  
[gpaules@mtpe.hq.nasa.gov](mailto:gpaules@mtpe.hq.nasa.gov)

##### Gene Trinh

Human Systems Research and Technology Division (ESMD)  
(202) 358-1490  
[eugene.h.trinh@nasa.gov](mailto:eugene.h.trinh@nasa.gov)

##### John Rush

Space Communications Office (SOMD)  
(202) 358-4819  
[john.j.rush@nasa.gov](mailto:john.j.rush@nasa.gov)





# TECH BRIEFS

NATIONAL AERONAUTICS AND SPACE ADMINISTRATION



## 5 Technology Focus: Sensors

- 5 Insect-Inspired Optical-Flow Navigation Sensors
- 6 Chemical Sensors Based on Optical Ring Resonators
- 7 A Broad-Band Phase-Contrast Wave-Front Sensor
- 8 Progress in Insect-Inspired Optical Navigation Sensors



## 11 Electronics/Computers

- 11 Portable Airborne Laser System Measures Forest-Canopy Height
- 11 Deployable Wide-Aperture Array Antennas
- 12 Faster Evolution of More Multifunctional Logic Circuits
- 13 Video-Camera-Based Position-Measuring System
- 14 N-Type  $\delta$  Doping of High-Purity Silicon Imaging Arrays



## 15 Software

- 15 Avionics System Architecture Tool
- 15 Updated Chemical Kinetics and Sensitivity Analysis Code
- 15 Predicting Flutter and Forced Response in Turbomachinery
- 15 Upgrades of Two Computer Codes for Analysis of Turbomachinery
- 16 Program Facilitates CMMI Appraisals
- 16 Grid Visualization Tool
- 16 Program Computes Sound Pressures at Rocket Launches
- 16 Solar-System Ephemeris Toolbox
- 16 Data-Acquisition Software for PSP/TSP Wind-Tunnel Cameras



## 19 Materials

- 19 Corrosion-Prevention Capabilities of a Water-Borne, Silicone-Based, Primerless Coating

- 19 Sol-Gel Process for Making Pt-Ru Fuel-Cell Catalysts

- 20 Making Activated Carbon for Storing Gas



## 21 Machinery/Automation

- 21 System Regulates the Water Contents of Fuel-Cell Streams
- 21 Five-Axis, Three-Magnetic-Bearing Dynamic Spin Rig



## 23 Manufacturing

- 23 Modifications of Fabrication of Vibratory Microgyroscopes



## 25 Bio-Medical

- 25 Chamber for Growing and Observing Fungi
- 25 Electroporation System for Sterilizing Water



## 27 Physical Sciences

- 27 Thermoelectric Air/Soil Energy-Harvesting Device
- 27 Flexible Metal-Fabric Radiators
- 28 Actuated Hybrid Mirror Telescope
- 29 Optical Design of an Optical Communications Terminal



## 31 Information Sciences

- 31 Algorithm for Identifying Erroneous Rain-Gauge Readings
- 31 Condition Assessment and End-of-Life Prediction System for Electric Machines and Their Loads



## 33 Books & Reports

- 33 Lightweight Thermal Insulation for a Liquid-Oxygen Tank
- 33 Stellar Gyroscope for Determining Attitude of a Spacecraft
- 33 Lifting Mechanism for the Mars Explorer Rover

This document was prepared under the sponsorship of the National Aeronautics and Space Administration. Neither the United States Government nor any person acting on behalf of the United States Government assumes any liability resulting from the use of the information contained in this document, or warrants that such use will be free from privately owned rights.



## Insect-Inspired Optical-Flow Navigation Sensors

Optical mouse chips are used to measure optical flow.

NASA's Jet Propulsion Laboratory, Pasadena, California

Integrated circuits that exploit optical flow to sense motions of computer mice on or near surfaces ("optical mouse chips") are used as navigation sensors in a class of small flying robots now undergoing development for potential use in such applications as exploration, search, and surveillance. The basic principles of these robots were described briefly in "Insect-Inspired Flight Control for Small Flying Robots" (NPO-30545), *NASA Tech Briefs*, Vol. 29, No. 1 (January 2005), page 61. To recapitulate from the cited prior article: The concept of optical flow can be defined, loosely, as the use of texture in images as a source of motion cues. The flight-control and navigation systems of these robots are inspired largely by the designs and functions of the vision systems and brains of insects, which have been demonstrated to utilize optical flow (as detected by their eyes and brains) resulting from their own motions in the environment.

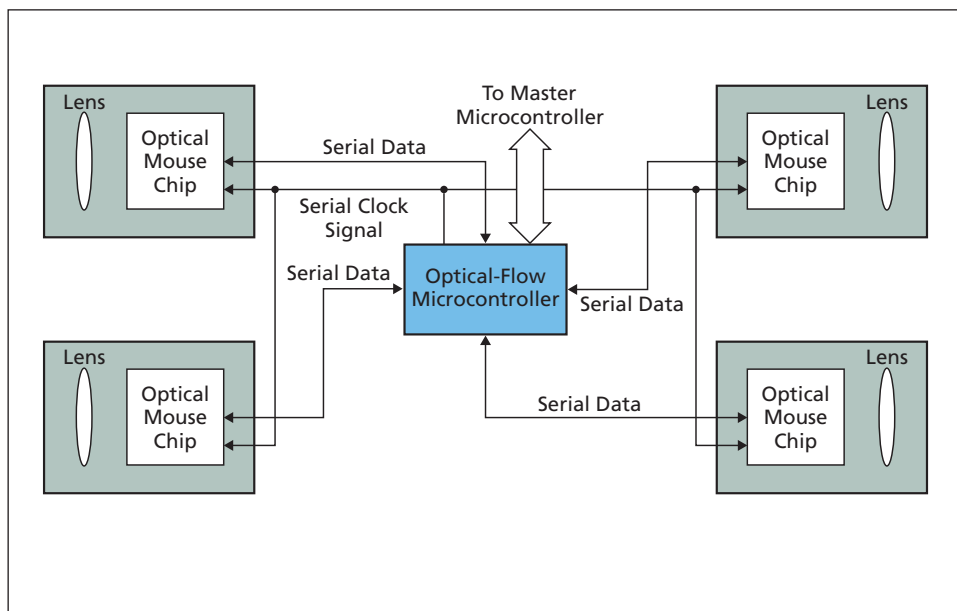
Optical flow has been shown to be very effective as a means of avoiding obstacles and controlling speeds and altitudes in robotic navigation. Prior systems used in experiments on navigating by means of optical flow have involved the use of panoramic optics, high-resolution image sensors, and programmable image-data-processing computers. These systems are large, complex, and computationally expensive, and not readily scalable for inclusion in miniature robots, for which there are severe design requirements to limit power demand, mass, and size.

The present development exploits the recent proliferation and commercial availability of optical mouse chips. Each optical mouse chip includes a low-resolution ( $16 \times 16$ ) array of photosensors, and circuitry that compares consecutive image frames to compute the optical flow across the array in two dimensions, in a manner analogous to that of an element in an insect's compound eye. In a com-

puter mouse, the optical flow is used to track the movement of the mouse on a mouse pad or equivalent surface; in a flying robot of the type now under development, the optical flow serves as a measure of two-dimensional velocity relative to nearby surfaces and objects. The use of optical mouse chips instead of the imaging-and-computing systems described above offers advantages of compactness, low mass (15 to 20 g per chip), low power

the information from each subsystem, and relay control information to affect locomotion. This hierarchical architecture is analogous to the neural structures of flies.

*This work was done by Sarita Thakoor and John M. Morookian of Caltech; Javan Chahl and Dean Soccol of Australian National University; and Butler Hine and Steven Zornetzer of NASA Ames Research Center for NASA's Jet Propulsion Labora-*



**Outputs of Optical Mouse Chips** would be fed to an optical-flow microcontroller for use in controlling a small flying robot. The number of mouse chips needed would increase with the required complexity of the behavior of the robot.

demand (42 mW per chip), low cost (about \$10 per chip in year 2004), redundancy, high speed (frame rates up to 2.3 kHz), and parallel processing.

In a hierarchical control architecture proposed for subsequent development of a flying robot, the outputs of several optical-mouse-type navigation sensors would be fed to a microcontroller (see figure) that would utilize the combined optical-flow information to determine the motion of the robot relative to the environment. This microcontroller would, in turn, communicate with a master microcontroller, which would combine information from various sensing subsystems, determine the priority to be assigned to

Further information is contained in a *TSP* (see page 1).

*In accordance with Public Law 96-517, the contractor has elected to retain title to this invention. Inquiries concerning rights for its commercial use should be addressed to:*

*Innovative Technology Assets Management  
JPL  
Mail Stop 202-233  
4800 Oak Grove Drive  
Pasadena, CA 91109-8099  
(818) 354-2240  
E-mail: iaoffice@jpl.nasa.gov*

*Refer to NPO-40173, volume and number of this NASA Tech Briefs issue, and the page number.*

# Chemical Sensors Based on Optical Ring Resonators

Resonance wavelengths are shifted by absorption of chemicals into polymer cladding layers.

NASA's Jet Propulsion Laboratory, Pasadena, California

Chemical sensors based on optical ring resonators are undergoing development. A ring resonator according to this concept is a closed-circuit dielectric optical waveguide. The outermost layer of this waveguide, analogous to the optical cladding layer on an optical fiber, is a made of a polymer that (1) has an index of refraction lower than that of the waveguide core and (2) absorbs chemicals from the surrounding air. The index of refraction of the polymer changes with the concentration of absorbed chemical(s). The resonator is designed to operate with relatively strong evanescent-wave coupling between the outer polymer layer and the electromagnetic field propagating along the waveguide core. By virtue of this coupling, the chemically induced change in index of refraction of the polymer causes a measurable shift in the resonance peaks of the ring.

In a prototype that has been used to demonstrate the feasibility of this sensor concept, the ring resonator is a dielectric optical waveguide laid out along a closed path resembling a racetrack (see Figure 1). The prototype was fabricated on a silicon substrate by use of standard techniques of thermal oxidation, chemical vapor deposition, photolithography, etching, and spin coating. The prototype resonator waveguide features an inner cladding of  $\text{SiO}_2$ , a core of  $\text{Si}_x\text{N}_y$ , and a chemical-sensing outer cladding of ethyl cellulose. In addition to the ring resonator, there are input and output waveguides separated from the straight segments of the ring resonator by an evanescent-wave-coupling gap of 2 mm.

Figure 2 presents results of a test of the prototype in an open room. During the test, the temperature of the sensor was stabilized to  $\pm 0.1$  K. The sensor was left undisturbed by chemicals, except during a short interval when a cotton swab wetted with isopropyl was placed 4 in. ( $\approx 10$  cm) away from the sensor and another short interval when a cotton swab wetted with acetone was similarly placed near the sensor. The chemical exposures resulted in easily detectable signals that exceeded background variations by at least an order of magnitude. The jagged nature of the portions of the plot corresponding to the chemical exposures has been attributed to "mode hops," in which the specific ring-resonator mode that was being followed moved out of the tuning range of a

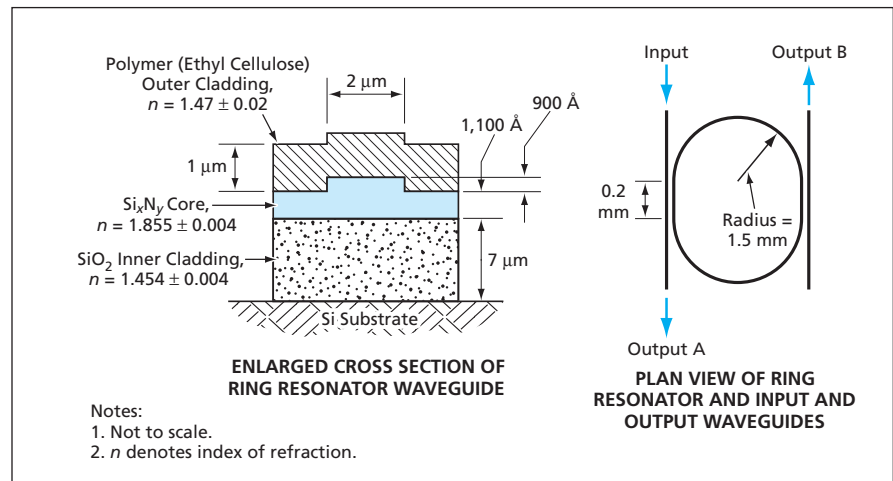


Figure 1. A Polymer-Clad Optical Ring Resonator acts as a chemical sensor in that the resonance spectrum becomes shifted in wavelength when the polymer absorbs chemicals from the air.

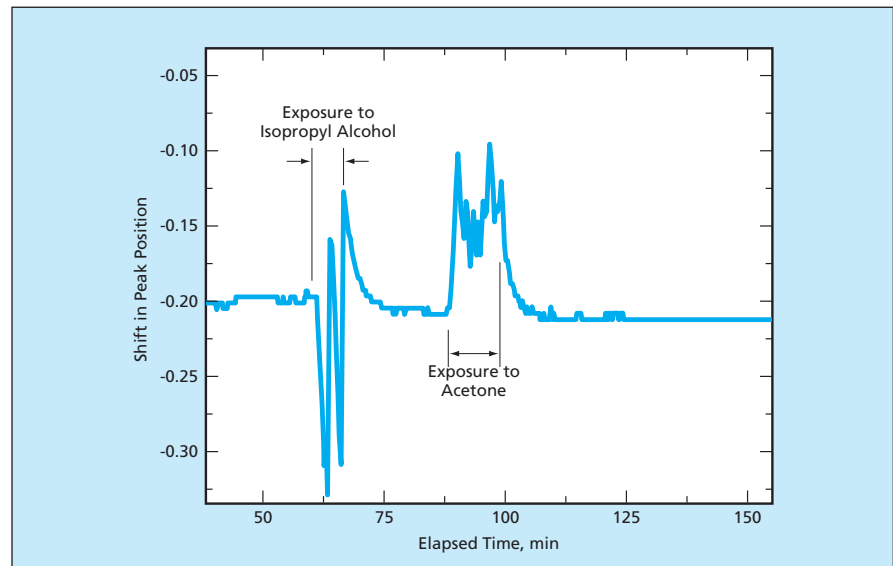


Figure 2. Shifts in the Wavelength of a peak in the resonance spectrum of the device of Figure 1 occurred during exposure to chemicals deliberately introduced into the air.

laser used as the input light source, causing the laser to lock onto a new mode.

The results have been interpreted as demonstrating the feasibility of optical polymer-based sensors. Inasmuch as the index of refraction of ethyl cellulose is known to respond to wide variety of volatiles, sensors like this one could be useful as non-specific indicators of spills of volatile compounds.

This work was done by Margie Homer, Allison Manfreda, Kamjou Mansour, Ying Lin, and Alexander Ksendzov of Caltech for NASA's Jet Propulsion Laboratory. Further information is contained in a TSP (see page 1).

In accordance with Public Law 96-517, the contractor has elected to retain title to this invention. Inquiries concerning rights for its commercial use should be addressed to:

Innovative Technology Assets Management  
JPL

Mail Stop 202-233  
4800 Oak Grove Drive  
Pasadena, CA 91109-8099  
(818) 354-2240

E-mail: iaoffice@jpl.nasa.gov

Refer to NPO-40601, volume and number of this NASA Tech Briefs issue, and the page number.

# A Broad-Band Phase-Contrast Wave-Front Sensor

The intrinsic  $90^\circ$  phase shift of an ideal beam splitter would be exploited.

NASA's Jet Propulsion Laboratory, Pasadena, California

A broadband phase-contrast wave-front sensor has been proposed as a real-time wave-front sensor in an adaptive-optics system. The proposed sensor would offer an alternative to the Shack-Hartmann wave-front sensors now used in high-order adaptive-optics systems of some astronomical telescopes. Broadband sensing gives higher sensitivity than does narrow-band sensing, and it appears that for a given bandwidth, the sensitivity of the proposed phase-contrast sensor could exceed that of a Shack-Hartmann sensor. Relative to a Shack-Hartmann sensor, the proposed sensor may be optically and mechanically simpler.

As described below, an important element of the principle of operation of a phase-contrast wave-front sensor is the imposition of a  $90^\circ$  phase shift between diffracted and undiffracted parts of the same light beam. In the proposed sensor, this phase shift would be obtained by utilizing the intrinsic  $90^\circ$  phase shift between the transmitted and reflected beams in an ideal (thin, symmetric) beam splitter. This phase shift can be characterized as achromatic or broadband because it is  $90^\circ$  at every wavelength over a broad wavelength range.

The phase-contrast approach was originally devised by Frits Zernike for microscopy as a means of obtaining intensity images from such phase objects as transparent biological samples. Figure 1 schematically illustrates an adaptation of the phase-contrast approach to real-time wave-front sensing for adaptive optics. The incident light from a guide star can be described in terms of a pupil field function  $A \exp(i\phi)$ , where  $A$  is an aperture function that expresses the effect of the shape and size of the telescope pupil and  $\phi$  is the difference between the actual instantaneous phase and the nominal (e.g., plane-wave) phase of the wave front at a given position within the pupil. If the pupil were simply re-imaged, the phase signal would not normally be observable. To make the phase signal observable, one reasons as follows:

Assuming a small-signal approximation ( $\phi \ll 1$ ), the phase part of the pupil field function could be approximated as  $1 + i\phi$ . Hence, the phase-difference (diffracted) component would be  $90^\circ$  out of phase with the larger undiffracted component. To a first approximation, the un-

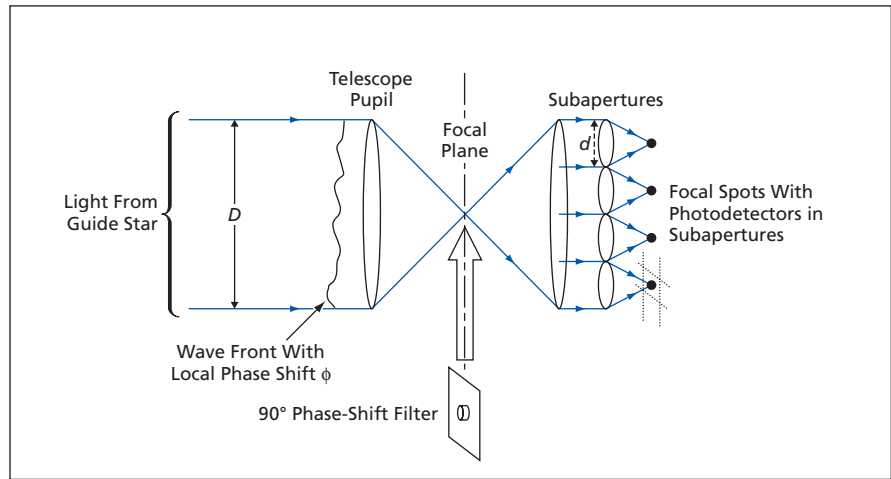


Figure 1. Phase-Contrast Imaging would use  $90^\circ$  phase shifting to generate phase feedback for adaptive optics.

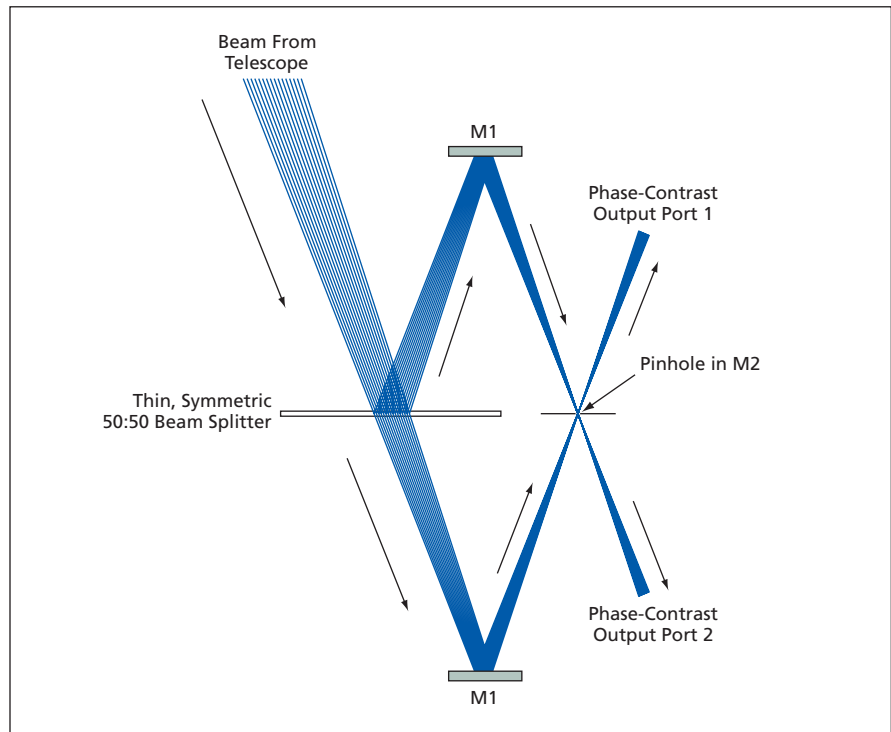


Figure 2. A Broad-Band Phase-Contrast Wave-Front Sensor, shown here schematically, can be realized by using the intrinsic properties of a beam splitter to give an achromatic  $90^\circ$ -phase-shifting element.

diffracted rays would be localized within the central  $\approx \lambda/D$  portion of the telescope focal plane (where  $\lambda$  is wavelength and  $D$  is the diameter of the primary mirror or lens of the telescope), while the diffracted rays that contribute to the phase component would impinge on the telescope focal plane at off-axis positions. If a  $\pm 90^\circ$ -phase-shift filter (e.g., a dielec-

tric disk of suitable thickness) having approximately the diffraction-limited size  $\lambda/D$  were placed at the focal point, then the undiffracted component would be shifted by  $\pm 90^\circ$  and would thereby be brought into phase (or phase opposition) with the diffracted component. As a result, the phase component would become observable as a small variation in

intensity across the pupil, superposed on the bright, uniform illumination of the undiffracted component. In the small-signal approximation, the total intensity in the re-imaged pupil would be proportional to  $1 \pm 2\phi$ , the sign of  $2\phi$  depending on whether the focal-spot filter advances or retards the phase.

Figure 2 schematically illustrates an optical assembly, according to the proposal, for implementing the  $90^\circ$ -phase-shift filter needed in a phase-contrast sensor like that of Figure 1. An incident beam from a telescope would strike a 50:50 beam splitter. The reflected and transmitted beams would be recombined by an arrangement of mirrors, schematically represented by flats M1 in Figure 2; one

component is directed through a diffraction-limited pinhole in two-sided mirror M2. The pinhole would pass the central  $\approx \lambda/D$  portions of the beams, while the M2 surfaces surrounding the pinhole would reflect the off-axis portions. The total beam going to the output port on each side of M2 would comprise the desired combination of central rays and  $90^\circ$ -shifted off-axis rays. The output beams could be directed into telescope-pupil-reimaging optics equipped with a charge-coupled-device (CCD) or similar quantum detector, as in Figure 1. Optionally, the phase-contrast images contained in both beams could be combined optically or electronically to increase the signal-to-noise ratio.

*This work was done by Eric Bloemhof and J. Kent Wallace of Caltech for NASA's Jet Propulsion Laboratory. Further information is contained in a TSP (see page 1).*

*In accordance with Public Law 96-517, the contractor has elected to retain title to this invention. Inquiries concerning rights for its commercial use should be addressed to:*

*Innovative Technology Assets Management  
JPL*

*Mail Stop 202-233  
4800 Oak Grove Drive  
Pasadena, CA 91109-8099  
(818) 354-2240*

*E-mail: iaoffice@jpl.nasa.gov*

*Refer to NPO-41401, volume and number of this NASA Tech Briefs issue, and the page number.*

## Progress in Insect-Inspired Optical Navigation Sensors

Some details of implementation have become available.

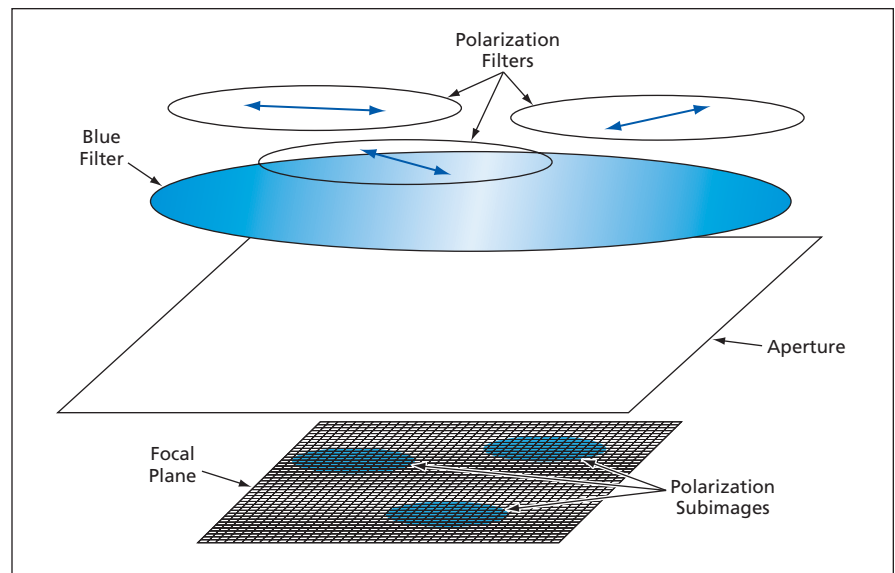
NASA's Jet Propulsion Laboratory, Pasadena, California

Progress has been made in continuing efforts to develop optical flight-control and navigation sensors for miniature robotic aircraft. The designs of these sensors are inspired by the designs and functions of the vision systems and brains of insects. Two types of sensors of particular interest are polarization compasses and ocellar horizon sensors.

The basic principle of polarization compasses was described (but without using the term "polarization compass") in "Insect-Inspired Flight Control for Small Flying Robots" (NPO-30545), *NASA Tech Briefs*, Vol. 29, No. 1 (January 2005), page 61. To recapitulate: Bees use sky polarization patterns in ultraviolet (UV) light, caused by Rayleigh scattering of sunlight by atmospheric gas molecules, as direction references relative to the apparent position of the Sun. A robotic direction-finding technique based on this concept would be more robust in comparison with a technique based on the direction to the visible Sun because the UV polarization pattern is distributed across the entire sky and, hence, is redundant and can be extrapolated from a small region of clear sky in an elsewhere cloudy sky that hides the Sun.

Three different implementations of a polarization compass are under consideration. Each implementation offers distinct advantages and disadvantages relative to the others:

- In the lightest and least power-consuming implementation, the polariza-



**Three Differently Oriented Polarization Filters** are used in projecting subimages on a CMOS image detector. In addition, a short-wavelength-pass (blue) filter contributes to image contrast because the polarization signal is strongest in blue light.

tion in the sky is sampled in, typically, 10 fields of view, each centered on a different direction and having an angular width between  $10^\circ$  and  $20^\circ$ . An eight-bit microcontroller suffices to do all required data processing. A production version of a sensor according to this implementation could be self-contained. One disadvantage of this implementation, as determined in experiments performed thus far, is that bearing accuracy is characterized by an uncertainty of about  $2^\circ$ . Another disadvan-

tage is that this sensor cannot be used for imaging.

- In the second implementation, three differently oriented polarization filters are used to produce three subimages of the sky scene in separate focal-plane areas of a complementary metal oxide/semiconductor (CMOS) video camera (see figure). This implementation is amenable to sophisticated processing of polarization-image data and possible sub-degree accuracy in determining the relative angular position of the Sun. Unfortunately, for a

production version, power consumption and mass would be much greater than in the first-mentioned implementation because an embedded computer or digital signal processor would be necessary for processing video data. Design and fabrication of the camera optics would present a challenge, inasmuch as the field of view should, ideally, be 150° wide. The challenge is compounded by the need to avoid reflective optics, which would disrupt the polarization pattern.

- In the most elegant implementation, not yet realized, each pixel of a charge-coupled-device (CCD) camera would be subdivided into three subpixels, each covered with a differently ori-

ented polarization filter. The resulting device would be small and lightweight and would demand little power, but manufacturing would be complex. The basic principle of ocellar horizon sensors was also described in the cited prior article. These sensors are based partly on dragonfly ocelli — simple eyes that exist in addition to the better-known compound eyes of insects and that sense only light, dark, and motion. In dragonflies, the ocelli play an important role in stabilizing attitude with respect to dorsal light levels.

An ocellar horizon sensor of the type under development includes UV/green pairs of photodiodes and utilizes drag-

onfly-inspired principles of color-opponency processing. The reason for choosing UV and green is that at these wavelengths, spectral sensitivity of dragonfly ocelli and the contrast between the sky and ground are greatest: On Earth, the contrast is greatest in the near UV during the day and is greatest in green at twilight.

*This work was done by Sarita Thakoor of Caltech, Javan Chahl of Australian National University, and Steve Zornetzer of NASA Ames Research Center for NASA's Jet Propulsion Laboratory. For further information, contact the JPL Innovative Partnerships Office at (818) 354-3821. NPO-41269*





## Portable Airborne Laser System Measures Forest-Canopy Height

This system can be built, operated, and repaired at relatively low cost.

Goddard Space Flight Center, Greenbelt, Maryland

The Portable Airborne Laser System (PALS) is a combination of laser ranging, video imaging, positioning, and data-processing subsystems designed for measuring the heights of forest canopies along linear transects from tens to thousands of kilometers long. Unlike prior laser ranging systems designed to serve the same purpose, the PALS is not restricted to use aboard a single aircraft of a specific type: the PALS fits into two large suitcases that can be carried to any convenient location, and the PALS can be installed in almost any local aircraft for hire, thereby making it possible to sample remote forests at relatively low cost. The initial cost and the cost of repairing the PALS are also lower because the PALS hardware consists mostly of commercial off-the-shelf (COTS) units

that can easily be replaced in the field.

The COTS units include a laser ranging transceiver, a charge-coupled-device camera that images the laser-illuminated targets, a differential Global Positioning System (dGPS) receiver capable of operation within the Wide Area Augmentation System, a video titler, a video cassette recorder (VCR), and a laptop computer equipped with two serial ports. The VCR and computer are powered by batteries; the other units are powered at 12 VDC from the 28-VDC aircraft power system via a low-pass filter and a voltage converter.

The dGPS receiver feeds location and time data, at an update rate of 0.5 Hz, to the video titler and the computer. The laser ranging transceiver, operating at a sampling rate of 2 kHz, feeds its serial

range and amplitude data stream to the computer. The analog video signal from the CCD camera is fed into the video titler wherein the signal is annotated with position and time information. The titler then forwards the annotated signal to the VCR for recording on 8-mm tapes. The dGPS and laser range and amplitude serial data streams are processed by software that displays the laser trace and the dGPS information as they are fed into the computer, subsamples the laser range and amplitude data, interleaves the subsampled data with the dGPS information, and records the resulting interleaved data stream.

*This work was done by Ross Nelson of Goddard Space Flight Center. Further information is contained in a TSP (see page 1). GSC-14906-1*

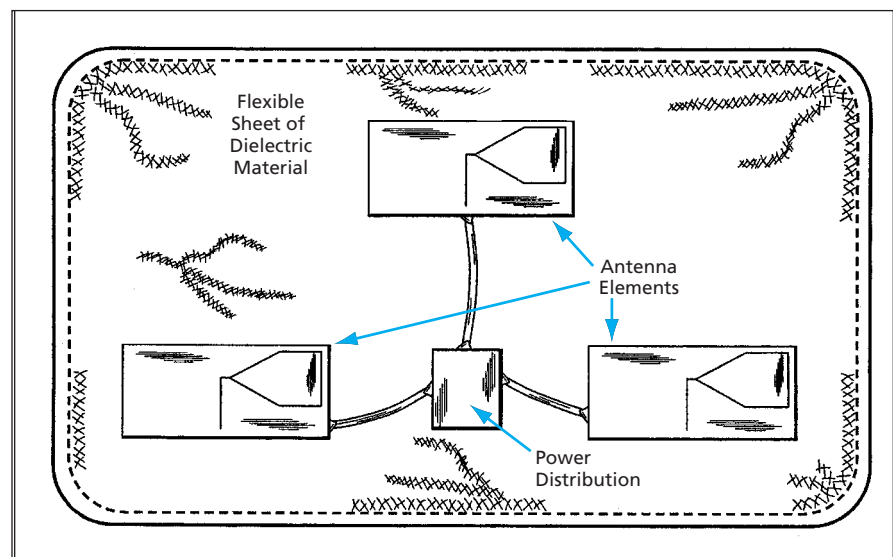
## Deployable Wide-Aperture Array Antennas

Antennas would be unrolled or unfolded to full size when and where needed.

Lyndon B. Johnson Space Center, Houston, Texas

Inexpensive, lightweight array antennas on flexible substrates are under development to satisfy a need for large-aperture antennas that can be stored compactly during transport and deployed to full size in the field. Conceived for use aboard spacecraft, antennas of this type also have potential terrestrial uses — most likely, as means to extend the ranges of cellular telephones in rural settings.

Several simple deployment mechanisms are envisioned. One example is shown in the figure, where the deployment mechanism, a springlike material contained in a sleeve around the perimeter of a flexible membrane, is based on a common automobile window shade. The array can be formed of antenna elements that are printed on small sections of semi-flexible laminates, or preferably, elements that are constructed of conducting fabric. Likewise,



A Wide Array of Four Radiating Antenna Elements and their transmission line would be made from flexible conductive materials on a flexible dielectric sheet. When not in use, the antenna could be rolled into a compact cylinder in the manner of a window shade.

a distribution network connecting the elements can be created from conventional technologies such as lightweight, flexible coaxial cable and a surface mount power divider, or preferably, from elements formed from conductive fabrics. Conventional technologies may be stitched onto a supporting flexible membrane or contained within pockets that are stitched onto a flexible membrane. Components created from conductive fabrics may be attached by stitching conductive strips to a nonconductive membrane, embroidering conductive threads into a nonconductive membrane, or weaving predetermined patterns directly into the membrane.

The deployable antenna may comprise multiple types of antenna elements. For example, thin profile antenna elements above a ground plane, both attached to the supporting flexible membrane, can be used to create a unidirectional boresight radiation pattern. Or, antenna elements without a ground plane, such as bow-tie dipoles, can be attached to the membrane to create a bidirectional array such as that shown in the figure. For either type of antenna element, the dual configuration, i.e., elements formed of slots in a conductive membrane, can also be used. Finally, wide bandwidth antennas or arrays can be formed in which the principal direc-

tion of radiation is in the plane of the membrane. For this embodiment, the set of elements on the membrane is arranged to form one or more traveling wave antennas. In this case, a nonconductive form of the perimeter springlike material is required to provide the deploying force.

*This work was done by Patrick W. Fink, Justin A. Dobbins, Greg Y. Lin, Andrew Chu, and Robert C. Scully of Johnson Space Center. This invention is owned by NASA, and a patent application has been filed. Inquiries concerning nonexclusive or exclusive license for its commercial development should be addressed to the Patent Counsel, Johnson Space Center, (281) 483-0837. Refer to MSC-23436.*

## Faster Evolution of More Multifunctional Logic Circuits

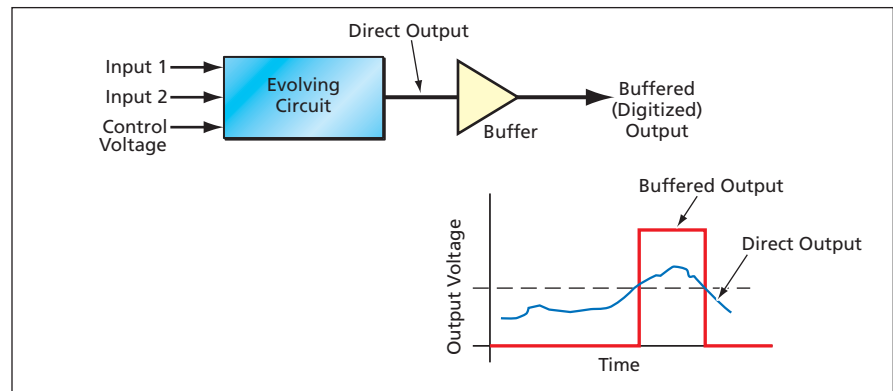
Evolution is driven to find circuits that perform larger numbers of logic functions.

NASA's Jet Propulsion Laboratory, Pasadena, California

A modification in a method of automated evolutionary synthesis of voltage-controlled multifunctional logic circuits makes it possible to synthesize more circuits in less time. Prior to the modification, the computations for synthesizing a four-function logic circuit by this method took about 10 hours. Using the method as modified, it is possible to synthesize a six-function circuit in less than half an hour.

The concepts of automated evolutionary synthesis and voltage-controlled multifunctional logic circuits were described in a number of prior *NASA Tech Briefs* articles. To recapitulate: A circuit is designed to perform one of several different logic functions, depending on the value of an applied control voltage. The circuit design is synthesized following an automated evolutionary approach that is so named because it is modeled partly after the repetitive trial-and-error process of biological evolution. In this process, random populations of integer strings that encode electronic circuits play a role analogous to that of chromosomes. An evolved circuit is tested by computational simulation (prior to testing in real hardware to verify a final design). Then, in a fitness-evaluation step, responses of the circuit are compared with specifications of target responses and circuits are ranked according to how close they come to satisfying specifications. The results of the evaluation provide guidance for refining designs through further iteration.

As described in more detail in the prior



**A Buffer Must Be Added** to an evolving circuit to obtain a digital output because the direct output of a typical evolving circuit is an analog voltage.

*NASA Tech Briefs* articles on multifunctional logic circuits, the multiple functionality of these circuits, the use of a single control voltage to select the function, and the automated evolutionary approach to synthesis, offer potential advantages for the further development of field-programmable gate arrays (FPGAs):

- Typical circuitry can be less complex and can occupy smaller areas; because only a single analog control line is needed to select different functions.
- If voltage-controlled multifunctional gates were used in the place of the configurable logic blocks of present commercial FPGAs, it would be possible to change the functions of the resulting digital systems in much shorter times;
- Relative to conventional circuits designed to perform single functions, multifunctional circuits can be synthe-

sized to be more tolerant of radiation-induced faults.

In the unmodified method of automated evolutionary synthesis, the target responses of a multifunctional logic circuit are fixed: that is, the user specifies in advance which logic function the circuit is to perform at each of several discrete values of control voltage (for example, AND at 0 V, NOR at 0.9 V, and NAND at 1.8 V). In the modified method, the user no longer specifies which logic function occurs at which control voltage: Instead, the evolutionary algorithm is allowed to find the control-voltage levels at which various logic functions appear, and the fitness-evaluation function is modified to assign a higher fitness score to a circuit that exhibits a greater number of logic functions over the full range of the control voltage. Thus, evolution is driven to

find circuits that perform a larger number of logic functions.

In order to be able to score fitness in this way, one must ensure that circuit output is a digital waveform at every value of the control voltage, so that the output can be classified as a particular logic function. Nevertheless, it has been observed that the circuits generated during evolu-

tionary search typically generate analog outputs, taking values between zero volts and the power-supply voltage. In order to solve this problem, the output of an evolving circuit is digitized by use of a buffer, as illustrated in the figure. Whereas the direct output of the evolving circuit is evaluated in the unmodified method, the buffered output is evaluated in the modi-

fied method. In effect, for the purpose of evaluation, the buffer becomes part of any such evolved circuit.

*This work was done by Adrian Stoica and Ricardo Zebulum of Caltech for NASA's Jet Propulsion Laboratory. Further information is contained in a TSP (see page 1). NPO-40934*

## Video-Camera-Based Position-Measuring System

Coordinates of nearby targeted objects are measured quickly, easily, and safely.

*John F. Kennedy Space Center, Florida*

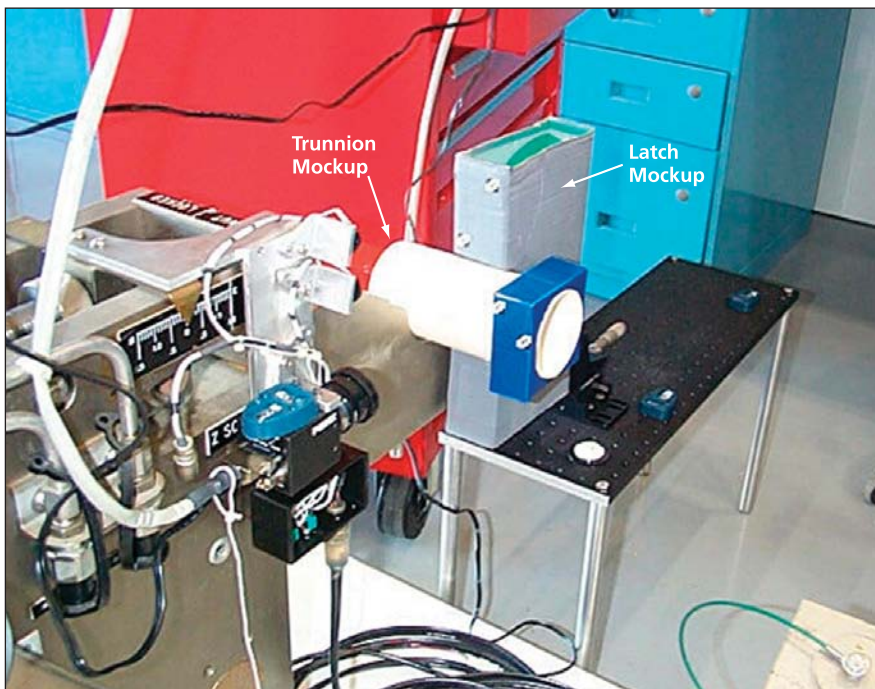


Figure 1. In this **Laboratory Setup**, the camera of the prototype system is aimed at a mockup of a latching with a trunnion to demonstrate the use of the system to measure the three-dimensional coordinates of the latch relative of the trunnion.

A prototype optoelectronic system measures the three-dimensional relative coordinates of objects of interest or of targets affixed to objects of interest in a workspace. The system includes a charge-coupled-device video camera mounted in a known position and orientation in the workspace, a frame grabber, and a personal computer running image-data-processing software. Relative to conventional optical surveying equipment, this system can be built and operated at much lower cost; however, it is less accurate. It is also much easier to operate than are conventional instrumentation systems. In addition, there is no need to establish a coordinate system through cooperative action by a team of surveyors.

The system operates in real time at around 30 frames per second (limited mostly by the frame rate of the camera). It continuously tracks targets as long as they remain in the field of the camera. In this respect, it emulates more expensive, elaborate laser tracking equipment that costs of the order of 100 times as much. Unlike laser tracking equipment, this system does not pose a hazard of laser exposure.

Images acquired by the camera are digitized and processed to extract all valid targets in the field of view. The three-dimensional coordinates ( $x$ ,  $y$ , and  $z$ ) of each target are computed from the pixel coordinates of the targets in the images to accuracy of the order of mil-

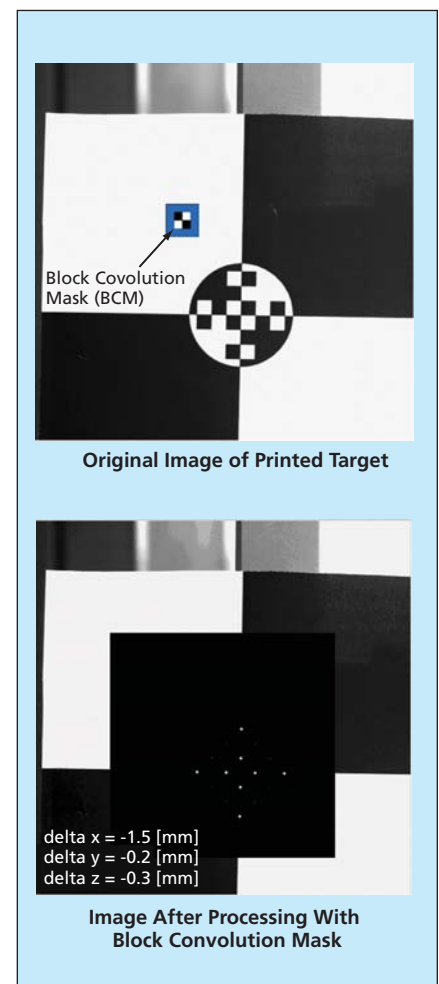


Figure 2. A **Target Pattern of Light and Dark Squares** is processed by a block convolution mask to obtain a pattern of bright dots on a dark background. The three-dimensional positions of the target can be determined from the pixel coordinates of the dots.

limeters over distances of the orders of meters. The system was originally intended specifically for real-time position measurement of payload transfers from payload canisters into the payload bay of

the Space Shuttle Orbiters (see Figure 1). The system may be easily adapted to other applications that involve similar coordinate-measuring requirements. Examples of such applications include manufacturing, construction, preliminary approximate land surveying, and aerial surveying.

For some applications with rectangular symmetry, it is feasible and desirable to attach a target composed of black and white squares to an object of interest (see Figure 2). For other situations,

where circular symmetry is more desirable, circular targets also can be created. Such a target can readily be generated and modified by use of commercially available software and printed by use of a standard office printer. All three relative coordinates ( $x$ ,  $y$ , and  $z$ ) of each target can be determined by processing the video image of the target. Because of the unique design of corresponding image-processing filters and targets, the vision-based position-measurement system is extremely

robust and tolerant of widely varying fields of view, lighting conditions, and varying background imagery.

*This work was done by John Lane, Christopher Immer, Jeffrey Brink, and Robert Youngquist of Dynacs, Inc. for Kennedy Space Center. For further information, contact:*

*Christopher Immer  
ASRC Aerospace  
Kennedy Space Center, FL 32899  
Phone No. (321) 867-6752  
KSC-12397/67/68/442*

## N-Type $\delta$ Doping of High-Purity Silicon Imaging Arrays Success depends on details of a low-temperature MBE process.

*NASA's Jet Propulsion Laboratory, Pasadena, California*

A process for n-type (electron-donor) delta ( $\delta$ ) doping has shown promise as a means of modifying back-illuminated image detectors made from n-doped high-purity silicon to enable them to detect high-energy photons (ultraviolet and x-rays) and low-energy charged particles (electrons and ions). This process is applicable to imaging detectors of several types, including charge-coupled devices, hybrid devices, and complementary metal oxide/semiconductor detector arrays.

Delta doping is so named because its density-vs.-depth characteristic is reminiscent of the Dirac  $\delta$  function (impulse function): the dopant is highly concentrated in a very thin layer. Preferably, the dopant is concentrated in one or at most two atomic layers in a crystal plane and, therefore,  $\delta$  doping is also known as atomic-plane doping. The use of  $\delta$  doping to enable detection of high-energy photons and low-energy particles was reported in several prior *NASA Tech Briefs* articles. As described in more detail in those articles, the main benefit afforded by  $\delta$  doping of a back-illuminated silicon detector is to eliminate a "dead" layer at the back surface of the silicon wherein high-energy photons and low-energy particles are absorbed without detection. An additional benefit is that the delta-doped layer can serve as a back-side electrical contact.

Delta doping of p-type silicon detectors is well established. The development of the present process addresses concerns specific to the  $\delta$  doping of high-purity silicon detectors, which are typically n-type. The present process involves relatively low temperatures, is fully compatible with other processes used to fabricate the detectors, and does not entail interruption of those processes. Indeed, this process can be the last stage in the fabrication of an imaging detector that has, in all other respects, already been fully processed, including metallized.

This process includes molecular-beam epitaxy (MBE) for deposition of three layers, including metallization. The success of the process depends on accurate temperature control, surface treatment, growth of high-quality crystalline silicon, and precise control of thicknesses of layers. MBE affords the necessary nanometer-scale control of the placement of atoms for delta doping.

More specifically, the process consists of MBE deposition of a thin silicon buffer layer, the n-type  $\delta$  doping layer, and a thin silicon cap layer. The n dopant selected for initial experiments was antimony, but other n dopants as (phosphorus or arsenic) could be used. All n-type dopants in silicon tend to

surface-segregate during growth, leading to a broadened dopant-concentration-versus-depth profile. In order to keep the profile as narrow as possible, the substrate temperature is held below 300 °C during deposition of the silicon cap layer onto the antimony delta layer. The deposition of silicon includes a silicon-surface-preparation step, involving H-termination, that enables the growth of high-quality crystalline silicon at the relatively low temperature with close to full electrical activation of donors in the surface layer.

*This work was done by Jordana Blacksborg, Michael Hoenk, and Shouleh Nikzad of Caltech for NASA's Jet Propulsion Laboratory. Further information is contained in a TSP (see page 1).*

*In accordance with Public Law 96-517, the contractor has elected to retain title to this invention. Inquiries concerning rights for its commercial use should be addressed to:*

*Innovative Technology Assets Management  
JPL  
Mail Stop 202-233  
4800 Oak Grove Drive  
Pasadena, CA 91109-8099  
(818) 354-2240  
E-mail: iaoffice@jpl.nasa.gov  
Refer to NPO-41166, volume and number of this NASA Tech Briefs issue, and the page number.*

## Avionics System Architecture Tool

Avionics System Architecture Tool (ASAT) is a computer program intended for use during the avionics-system-architecture-design phase of the process of designing a spacecraft for a specific mission. ASAT enables simulation of the dynamics of the command-and-data-handling functions of the spacecraft avionics in the scenarios in which the spacecraft is expected to operate. ASAT is built upon I-Logix Statemate MAGNUM, providing a complement of dynamic system modeling tools, including a graphical user interface (GUI), modeling checking capabilities, and a simulation engine. ASAT augments this with a library of predefined avionics components and additional software to support building and analyzing avionics hardware architectures using these components.

*This program was written by Savio Chau, Ronald Hall, and Marcus Traylor of Caltech, and Adrian Whitfield of I-Logix for NASA's Jet Propulsion Laboratory. Further information is contained in a TSP (see page 1).*

*This software is available for commercial licensing. Please contact Karina Edmonds of the California Institute of Technology at (818) 393-2827. Refer to NPO-30629.*

## Updated Chemical Kinetics and Sensitivity Analysis Code

An updated version of the General Chemical Kinetics and Sensitivity Analysis (LSENS) computer code has become available. A prior version of LSENS was described in "Program Helps to Determine Chemical-Reaction Mechanisms" (LEW-15758), *NASA Tech Briefs*, Vol. 19, No. 5 (May 1995), page 66. To recapitulate: LSENS solves complex, homogeneous, gas-phase, chemical-kinetics problems (e.g., combustion of fuels) that are represented by sets of many coupled, nonlinear, first-order ordinary differential equations. LSENS has been designed for flexibility, convenience, and computational efficiency. The present version of LSENS incorporates mathematical models for (1) a static system; (2) steady, one-dimensional inviscid flow; (3) reaction behind an incident shock wave, including boundary-layer correction; (4) a perfectly stirred reactor; and (5) a perfectly stirred reactor followed by a plug-flow reactor. In addition,

LSENS can compute equilibrium properties for the following assigned states: enthalpy and pressure, temperature and pressure, internal energy and volume, and temperature and volume. For static and one-dimensional-flow problems, including those behind an incident shock wave and following a perfectly stirred reactor calculation, LSENS can compute sensitivity coefficients of dependent variables and their derivatives, with respect to the initial values of dependent variables and/or the rate-coefficient parameters of the chemical reactions.

*This program was written by Krishnan Radhakrishnan of the Institute for Computational Mechanics in Propulsion for Glenn Research Center. Further information is contained in a TSP (see page 1).*

*Inquiries concerning rights for the commercial use of this invention should be addressed to NASA Glenn Research Center, Commercial Technology Office, Attn: Steve Fedor, Mail Stop 4-8, 21000 Brookpark Road, Cleveland, Ohio 44135. Refer to LEW-17519-1.*

## Predicting Flutter and Forced Response in Turbomachinery

TURBO-AE is a computer code that enables detailed, high-fidelity modeling of aeroelastic and unsteady aerodynamic characteristics for prediction of flutter, forced response, and blade-row interaction effects in turbomachinery. Flow regimes that can be modeled include subsonic, transonic, and supersonic, with attached and/or separated flow fields. The three-dimensional Reynolds-averaged Navier-Stokes equations are solved numerically to obtain extremely accurate descriptions of unsteady flow fields in multistage turbomachinery configurations. Blade vibration is simulated by use of a dynamic-grid-deformation technique to calculate the energy exchange for determining the aerodynamic damping of vibrations of blades. The aerodynamic damping can be used to assess the stability of a blade row. TURBO-AE also calculates the unsteady blade loading attributable to such external sources of excitation as incoming gusts and blade-row interactions. These blade loadings, along with aerodynamic damping, are used to calculate the forced responses of blades to predict their fatigue lives. Phase-lagged boundary conditions based on the direct-store

method are used to calculate nonzero interblade phase-angle oscillations; this practice eliminates the need to model multiple blade passages, and, hence, enables large savings in computational resources.

*This program was written by Dale E. VanZante and John J. Adamczyk of Glenn Research Center; Rakesh Srivastava, Milind A. Bakhle, and Aamir Shabbir of the University of Toledo; Jen-Ping Chen and J. Mark Janus of Mississippi State University; Wai-Ming To of AP Solutions, Inc.; and John Barter of GE Aircraft Engines. Further information is contained in a TSP (see page 1).*

*Inquiries concerning rights for the commercial use of this invention should be addressed to NASA Glenn Research Center, Commercial Technology Office, Attn: Steve Fedor, Mail Stop 4-8, 21000 Brookpark Road, Cleveland, Ohio 44135. Refer to LEW-17514-1.*

## Upgrades of Two Computer Codes for Analysis of Turbomachinery

Major upgrades have been made in two of the programs reported in "Five Computer Codes for Analysis of Turbomachinery" (LEW-16851), *NASA Tech Briefs*, Vol. 23, No. 11 (November 1999), page 28. The affected programs are:

- Swift — a code for three-dimensional (3D) multiblock analysis; and
- TCGRID, which generates a 3D grid used with Swift.

Originally utilizing only a central-differencing scheme for numerical solution, Swift was augmented by addition of two upwind schemes that give greater accuracy but take more computing time. Other improvements in Swift include addition of a shear-stress-transport turbulence model for better prediction of adverse pressure gradients, addition of an H-grid capability for flexibility in modeling flows in pumps and ducts, and modification to enable simultaneous modeling of hub and tip clearances. Improvements in TCGRID include modifications to enable generation of grids for more complicated flow paths and addition of an option to generate grids compatible with the ADPAC code used at NASA and in industry. For both codes, new test cases were developed and documentation was updated. Both codes were converted to Fortran 90, with dynamic memory allocation. Both codes were also modified for ease of use in

both UNIX and Windows operating systems.

*These programs were written by Rodrick V. Chima and Meng-Sing Liou of Glenn Research Center. Further information is contained in a TSP (see page 1).*

*Inquiries concerning rights for the commercial use of this invention should be addressed to NASA Glenn Research Center, Commercial Technology Office, Attn: Steve Fedor, Mail Stop 4-8, 21000 Brookpark Road, Cleveland, Ohio 44135. Refer to LEW-17635/88-1.*

---

## Program Facilitates CMMI Appraisals

A computer program has been written to facilitate appraisals according to the methodology of Capability Maturity Model Integration (CMMI). [CMMI is a government/industry standard, maintained by the Software Engineering Institute at Carnegie Mellon University, for objectively assessing the engineering capability and maturity of an organization (especially, an organization that produces software)]. The program assists in preparation for a CMMI appraisal by providing drop-down lists suggesting required artifacts or evidence. It identifies process areas for which similar evidence is required and includes a copy feature that reduces or eliminates repetitive data entry. It generates reports to show the entire framework for reference, the appraisal artifacts to determine readiness for an appraisal, and lists of interviewees and questions to ask them during the appraisal. During an appraisal, the program provides screens for entering observations and ratings, and reviewing evidence provided thus far. Findings concerning strengths and weaknesses can be exported for use in a report or a graphical presentation. The program generates a chart showing capability level ratings of the organization. A context-sensitive Windows help system enables a novice to use the program and learn about the CMMI appraisal process.

*This program was written by Wesley Sweetser of Goddard Space Flight Center. Further information is contained in a TSP (see page 1). GSC-14782-1*

---

## Grid Visualization Tool

The Grid Visualization Tool (GVT) is a computer program for displaying the path of a mobile robotic explorer (rover) on a terrain map. The GVT reads a map-data file in either portable graymap (PGM) or portable pixmap (PPM) format, representing a gray-scale

or color map image, respectively. The GVT also accepts input from path-planning and activity-planning software. From these inputs, the GVT generates a map overlaid with one or more rover path(s), waypoints, locations of targets to be explored, and/or target-status information (indicating success or failure in exploring each target). The display can also indicate different types of paths or path segments, such as the path actually traveled versus a planned path or the path traveled to the present position versus planned future movement along a path. The program provides for updating of the display in real time to facilitate visualization of progress. The size of the display and the map scale can be changed as desired by the user. The GVT was written in the C++ language using the Open Graphics Library (OpenGL) software. It has been compiled for both Sun Solaris and Linux operating systems.

*This program was written by Caroline Chouinard, Forest Fisher, Tara Estlin, Daniel Gaines, and Steven Schaffer of Caltech for NASA's Jet Propulsion Laboratory. Further information is contained in a TSP (see page 1).*

*This software is available for commercial licensing. Please contact Karina Edmonds of the California Institute of Technology at (818) 393-2827. Refer to NPO-40303.*

---

## Program Computes Sound Pressures at Rocket Launches

Launch Vehicle External Sound Pressure is a computer program that predicts the ignition overpressure and the acoustic pressure on the surfaces and in the vicinity of a rocket and launch pad during launch. The program generates a graphical user interface (GUI) that gathers input data from the user. These data include the critical dimensions of the rocket and of any launch-pad structures that may act as acoustic reflectors, the size and shape of the exhaust duct or flame deflector, and geometrical and operational parameters of the rocket engine. For the ignition-overpressure calculations, histories of the chamber pressure and mass flow rate also are required. Once the GUI has gathered the input data, it feeds them to ignition-overpressure and launch-acoustics routines, which are based on several approximate mathematical models of distributed sources, transmission, and reflection of acoustic waves. The out-

put of the program includes ignition overpressures and acoustic pressures at specified locations.

*This program was written by Gary Ogg, Roy Heyman, Michael White, and Karl Edquist of Applied Research Associates, Inc., for Marshall Space Flight Center. For further information, contact the company at [www.ara.com](http://www.ara.com). MFS-31568*

---

## Solar-System Ephemeris Toolbox

NASA's Jet Propulsion Laboratory (JPL) generates planetary and lunar ephemeris data and FORTRAN routines that allow users to obtain state data for the Sun, the moon, and the planets. The JPL Solar System Ephemeris Toolbox, developed at Kennedy Space Center, is a set of functions that provides the same functionality in the MATLAB computing environment along with some additional capabilities. The toolbox can be used interactively via a graphical user interface (GUI), or individual functions can be called from the MATLAB command prompt or other MATLAB scripts and functions. The toolbox also includes utility functions to define and perform coordinate transformation (e.g., mean-of-date, true-of-date, J2000) that are common in the use of these ephemerides. An attached README file guides the user through the process of constructing binary ephemeris files, verifying correct installation, and using functions to extract state data. This process also can be performed using the GUI. Help from each toolbox function is available through MATLAB's "help" function. Many of the functions in the toolbox are MATLAB equivalents of the JPL-written FORTRAN programs and sub-routines used for the same purposes. A novice can use the GUI to extract state data, while a more experienced user can use the functions directly, as needed, in his/her applications. The toolbox has been tested using MATLAB Releases 13 and 14.

*This program was written by Charles F. Walker of Kennedy Space Center. For further information, access [www.openchannelsoftware.org](http://www.openchannelsoftware.org). KSC-12544*

---

## Data-Acquisition Software for PSP/TSP Wind-Tunnel Cameras

Wing-Viewer is a computer program for acquisition and reduction of image data acquired by any of five different scientific-grade commercial electronic cameras used at Langley Research center to observe wind-tunnel models coated with pressure-

or temperature-sensitive paints (PSP/TSP). Wing-Viewer provides full automation of camera operation and acquisition of image data, and has limited data-preprocessing capability for quick viewing of the results of PSP/TSP test images. Wing-Viewer satisfies a requirement for a standard interface between all the cameras

and a single personal computer: Written by use of Microsoft Visual C++ and the Microsoft Foundation Class Library as a framework, Wing-Viewer has the ability to communicate with the C/C++ software libraries that run on the controller circuit cards of all five cameras. Wing-Viewer saves image data in tagged image file

(TIF) version 6.0 format. Wing-Viewer can function on computers that run any of the several Windows operating systems, including Windows 95, 98, 2000, and NT.

*This program was written by Tahani R. Amer and William K. Goad of **Langley Research Center**. Further information is contained in a TSP (see page 1). LAR-16474-1*





## Corrosion-Prevention Capabilities of a Water-Borne, Silicone-Based, Primerless Coating

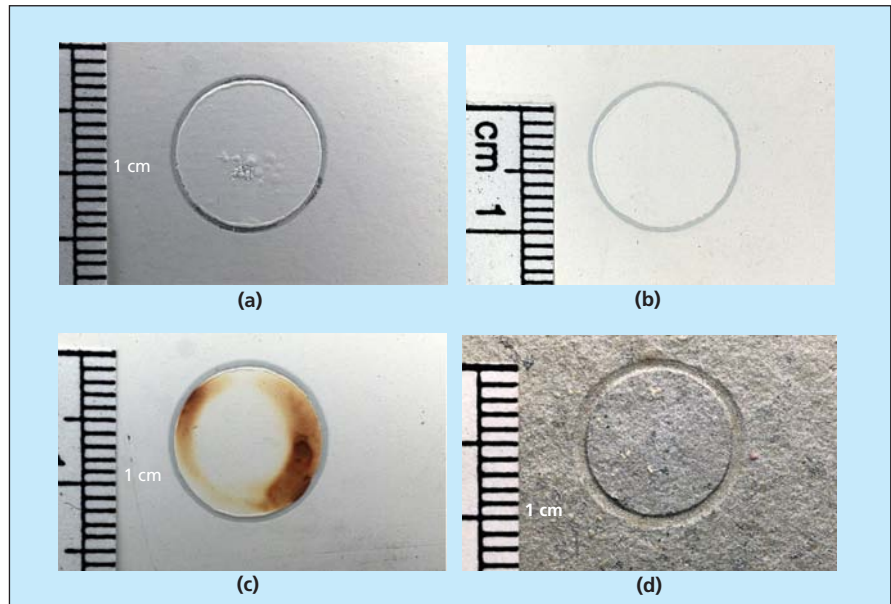
Some formulations are better for steel, some for aluminum.

John F. Kennedy Space Center, Florida

Comparative tests have been performed to evaluate the corrosion-prevention capabilities of an experimental paint of the type described in "Water-Borne, Silicone-Based, Primerless Paints," *NASA Tech Briefs*, Vol. 26, No. 11 (November 2002), page 30. To recapitulate: these paints contain relatively small amounts of volatile organic solvents and were developed as substitutes for traditional anti-corrosion paints that contain large amounts of such solvents. An additional desirable feature of these paints is that they can be applied without need for prior application of primers to ensure adhesion.

The test specimens included panels of cold-rolled steel, stainless steel 316, and aluminum 2024-T3. Some panels of each of these alloys were left bare and some were coated with the experimental water-borne, silicone-based, primerless paint. In addition, some panels of aluminum 2024-T3 and some panels of a fourth alloy (stainless steel 304) were coated with a commercial solvent-borne paint containing aluminum and zinc flakes in a nitrile rubber matrix. In the tests, the specimens were immersed in an aerated 3.5-weight-percent aqueous solution of NaCl for 168 hours. At intervals of 24 hours, the specimens were characterized by electrochemical impedance spectroscopy (EIS) and measurements of corrosion potentials. The specimens were also observed visually.

As indicated by photographs of specimens taken after the 168-hour immersion



**Blistering of an Experimental Silicone Paint** is manifest on two alloy specimens after immersion for a week in an aerated saltwater solution: (a) silicone-coated aluminum 2024-T3 panel, (b) silicone-coated 316 stainless-steel panel, (c) silicone-coated cold-rolled-steel panel, and (d) aluminum 2024-T3 panel coated with aluminum- and zinc-filled nitrile rubber.

(see figure), the experimental primerless silicone paint was effective in preventing corrosion of stainless steel 316, but failed to protect aluminum 2024-T3 and cold-rolled steel. The degree of failure was greater in the case of the cold-rolled steel. On the basis of visual observations, EIS, and corrosion-potential measurements, it was concluded that the commercial aluminum- and zinc-filled nitrile rubber coating affords

superior corrosion protection to aluminum 2024-T3 and is somewhat less effective in protecting stainless steel 304.

*This work was done by Luz Marina Calle and Louis G. MacDowell of Kennedy Space Center, and Rubie D. Vinje of ASRC Aerospace. For further information, contact the Kennedy Innovative Partnerships Office at (321) 867-1463. KSC-12520*

## Sol-Gel Process for Making Pt-Ru Fuel-Cell Catalysts

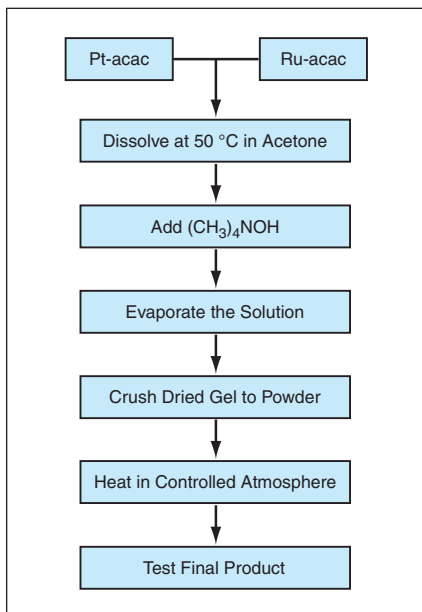
Relative to another process, this one takes less time and yields better results.

NASA's Jet Propulsion Laboratory, Pasadena, California

A sol-gel process has been developed as a superior alternative to a prior process for making platinum-ruthenium alloy catalysts for electro-oxidation of methanol in fuel cells. The starting materials in the prior process are chloride salts of platinum and ruthenium. The

process involves multiple steps, is time-consuming, and yields a Pt-Ru product that has relatively low specific surface area and contains some chloride residue. Low specific surface area translates to incomplete utilization of the catalytic activity that might otherwise be available,

while chloride residue further reduces catalytic activity ("poisons" the catalyst). In contrast, the sol-gel process involves fewer steps and less time, does not leave chloride residue, and yields a product of greater specific area and, hence, greater catalytic activity.



**Pt-Ru Catalytic Powder Is Made** from organic salts of Pt and Ru in a sol-gel process that involves fewer steps and less time than does a process based on chloride salts of Pt and Ru.

In this sol-gel process (see figure), the starting materials are platinum(II) acetylacetonate [Pt(C<sub>5</sub>H<sub>7</sub>O<sub>2</sub>)<sub>2</sub>, also denoted Pt-acac] and ruthenium(III) acetylacetonate [Ru(C<sub>5</sub>H<sub>7</sub>O<sub>2</sub>)<sub>3</sub>, also denoted Ru-acac]. First, Pt-acac and Ru-acac are dis-

solved in acetone at the desired concentrations (typically, 0.00338 moles of each salt per 100 mL of acetone) at a temperature of 50 °C. A solution of 25 percent tetramethylammonium hydroxide [(CH<sub>3</sub>)<sub>4</sub>NOH, also denoted TMAH] in methanol is added to the Pt-acac/Ru-acac/acetone solution to act as a high-molecular-weight hydrolyzing agent. The addition of the TMAH counteracts the undesired tendency of Pt-acac and Ru-acac to precipitate as separate phases during the subsequent evaporation of the solvent, thereby helping to yield a desired homogeneous amorphous gel. The solution is stirred for 10 minutes, then the solvent is evaporated until the solution becomes viscous, eventually transforming into a gel. The viscous gel is dried in air at a temperature of 170 °C for about 10 hours. The dried gel is crushed to make a powder that is the immediate precursor of the final catalytic product.

The precursor powder is converted to the final product in a controlled-atmosphere heat treatment. Desirably, the final product is a phase-pure (Pt phase only) Pt-Ru powder with a high specific surface area. The conditions of the controlled-atmosphere heat are critical for obtaining the aforementioned desired

properties. A typical heat treatment that yields best results for a catalytic alloy of equimolar amounts of Pt and Ru consists of at least two cycles of heating to a temperature of 300 °C and holding at 300 °C for several hours, all carried out in an atmosphere of 1 percent O<sub>2</sub> and 99 percent N<sub>2</sub>. The resulting powder consists of crystallites with typical linear dimensions of <10 nm. Tests have shown that the powder is highly effective in catalyzing the electro-oxidation of methanol.

*This work was done by Sekharipuram Narayanan and Thomas Valdez of Caltech, and Prashant Kumta and Y. Kim of Carnegie-Mellon University for NASA's Jet Propulsion Laboratory. Further information is contained in a TSP (see page 1).*

*In accordance with Public Law 96-517, the contractor has elected to retain title to this invention. Inquiries concerning rights for its commercial use should be addressed to:*

*Innovative Technology Assets Management:*

*JPL*

*Mail Stop 202-233*

*4800 Oak Grove Drive*

*Pasadena, CA 91109-8099*

*(818) 354-2240*

*E-mail: iaoffice@jpl.nasa.gov*

*Refer to NPO-30500, volume and number of this NASA Tech Briefs issue, and the page number.*

## Making Activated Carbon for Storing Gas

*Lyndon B. Johnson Space Center, Houston, Texas*

Solid disks of microporous activated carbon, produced by a method that enables optimization of pore structure, have been investigated as means of storing gas (especially hydrogen for use as a fuel) at relatively low pressure through adsorption on pore surfaces. For hydrogen and other gases of practical interest, a narrow distribution of pore sizes <2 nm is preferable. The present method is a variant of a previously patented method of cyclic chemisorption and desorption in which a piece of carbon

is alternately (1) heated to the lower of two elevated temperatures in air or other oxidizing gas, causing the formation of stable carbon/oxygen surface complexes; then (2) heated to the higher of the two elevated temperatures in flowing helium or other inert gas, causing the desorption of the surface complexes in the form of carbon monoxide. In the present method, pore structure is optimized partly by heating to a temperature of 1,100 °C during carbonization. Another aspect of the method exploits

the finding that for each gas-storage pressure, gas-storage capacity can be maximized by burning off a specific proportion (typically between 10 and 20 weight percent) of the carbon during the cyclic chemisorption/desorption process.

*This work was done by Marek A. Wójtowicz and Michael A. Serio of Advanced Fuels Research, Inc., and Eric M. Suuberg (consultant) for Johnson Space Center. For further information, contact the Johnson Innovative Partnerships Office at (281) 483-3809. MSC-23233*



## System Regulates the Water Contents of Fuel-Cell Streams

Lyndon B. Johnson Space Center, Houston, Texas

An assembly of devices provides for both humidification of the reactant gas streams of a fuel cell and removal of the product water (the water generated by operation of the fuel cell). The assembly includes externally-sensing forward-pressure regulators that supply reactant gases (fuel and oxygen) at variable pressures to ejector reactant pumps. The ejector supply pressures depend on the consumption flows. The ejectors develop differential pressures approximately

proportional to the consumption flow rates at constant system pressure and with constant flow restriction between the mixer-outlet and suction ports of the ejectors. For removal of product water from the circulating oxygen stream, the assembly includes a water/gas separator that contains hydrophobic and hydrophilic membranes. The water separator imposes an approximately constant flow restriction, regardless of the quality of the two-phase flow that enters it from the

fuel cell. The gas leaving the water separator is nearly 100 percent humid. This gas is returned to the inlet of the fuel cell along with a quantity of dry incoming oxygen, via the oxygen ejector, thereby providing some humidification.

*This work was done by Arturo Vasquez and Scott Lazaroff of Johnson Space Center. For further information, contact the Johnson Innovative Partnerships Office at (281) 483-3809. MSC-23079*

## Five-Axis, Three-Magnetic-Bearing Dynamic Spin Rig

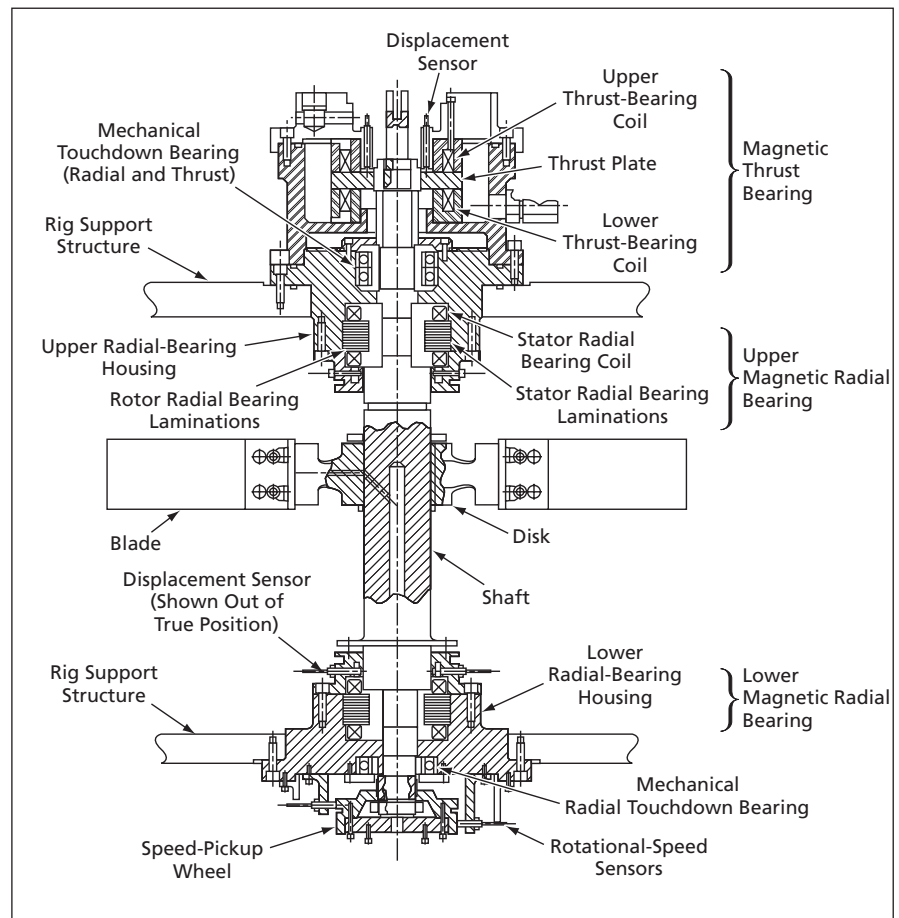
Higher-order vibrational modes can be excited and higher rotational speeds attained.

John H. Glenn Research Center, Cleveland, Ohio

The Five-Axis, Three-Magnetic-Bearing Dynamic Spin Rig is an apparatus for vibration testing of turbomachine blades in a vacuum at rotational speeds from 0 to 40,000 rpm. This rig (see figure) includes (1) a vertically oriented shaft on which is mounted an assembly comprising a rotor holding the blades to be tested, (2) two actively controlled heteropolar radial magnetic bearings at opposite ends of the shaft, and (3) an actively controlled magnetic thrust bearing at the upper end of the shaft. This rig is a more capable successor to a prior apparatus, denoted the Dynamic Spin Rig (DSR), that included a vertically oriented shaft with a mechanical thrust bearing at the upper end and a single actively controlled heteropolar radial magnetic bearing at the lower end.

The five-axis, three-magnetic-bearing configuration of the present rig enables full magnetic suspension of the rotor — eliminating mechanical contact between the rotor and the bearings during operation. Whereas frictional heating in the mechanical thrust bearing of the prior DSR made it necessary to limit rotational speed to 18,000 rpm or less, the absence of frictional heating in the present rig makes it possible to operate at higher speed, provided that a rotor of appropriate high-speed design is installed.

In the prior DSR, it was not possible to excite vibrations in higher-order modes in bladed-disk test assemblies by



The **Five-Axis, Three-Magnetic-Bearing** configuration of this dynamic spin rig makes it possible to excite high-order vibrational modes of the disk-and-blade assembly. The five axes are the vertical thrust axis of the thrust bearing and two mutually perpendicular horizontal force axes for each of the two radial bearings.

applying feed-forward control excitations to the magnetic bearings. This limitation was due partly to the lateral constraint imposed on the rotor by the mechanical bearing at the upper end of the shaft, partly to the direct effect of friction in that bearing, and partly to the aforementioned speed limit imposed to prevent excessive frictional heating. In contrast, by virtue of the fully magnetic nature of the present suspension, there is no lateral constraint against vibrations, and excitation ampli-

tudes can be greater than in the prior DSR. By applying appropriate feed-forward bounce-mode and tilt-mode control excitation command to the active magnetic bearings in the present rig, one can excite vibrations in a variety of modes. The combination of large-amplitude feed-forward excitation and higher rotational speed makes it possible to excite higher-order vibrations in a bladed-disk test assembly.

*This work was done by Carlos R. Morrison, Andrew Provenza, Anatole Kurkov, Oral*

*Mehmed, and Dexter Johnson of **Glenn Research Center**; Gerald Montague of The Army Research Laboratory; and Kirsten Duffy and Ralph Jansen of The University of Toledo. Further information is contained in a TSP (see page 1).*

*Inquiries concerning rights for the commercial use of this invention should be addressed to NASA Glenn Research Center, Innovative Partnerships Office, Attn: Steve Fedor, Mail Stop 4-8, 21000 Brookpark Road, Cleveland, Ohio 44135. Refer to LEW-17757-1.*

## Modifications of Fabrication of Vibratory Microgyroscopes

The goal is to increase production yields.

NASA's Jet Propulsion Laboratory, Pasadena, California

A micromachining process for the fabrication of vibratory microgyroscopes from silicon wafers, and aspects of the microgyroscope design that are inextricably linked with the fabrication process, have been modified in an effort to increase production yields from perspectives of both quantity and quality.

Prior to the modifications, the effective production yield of working microgyroscopes was limited to one or less per wafer. The modifications are part of a continuing effort to improve the design and increase production yields to more than 30 working microgyroscopes per wafer.

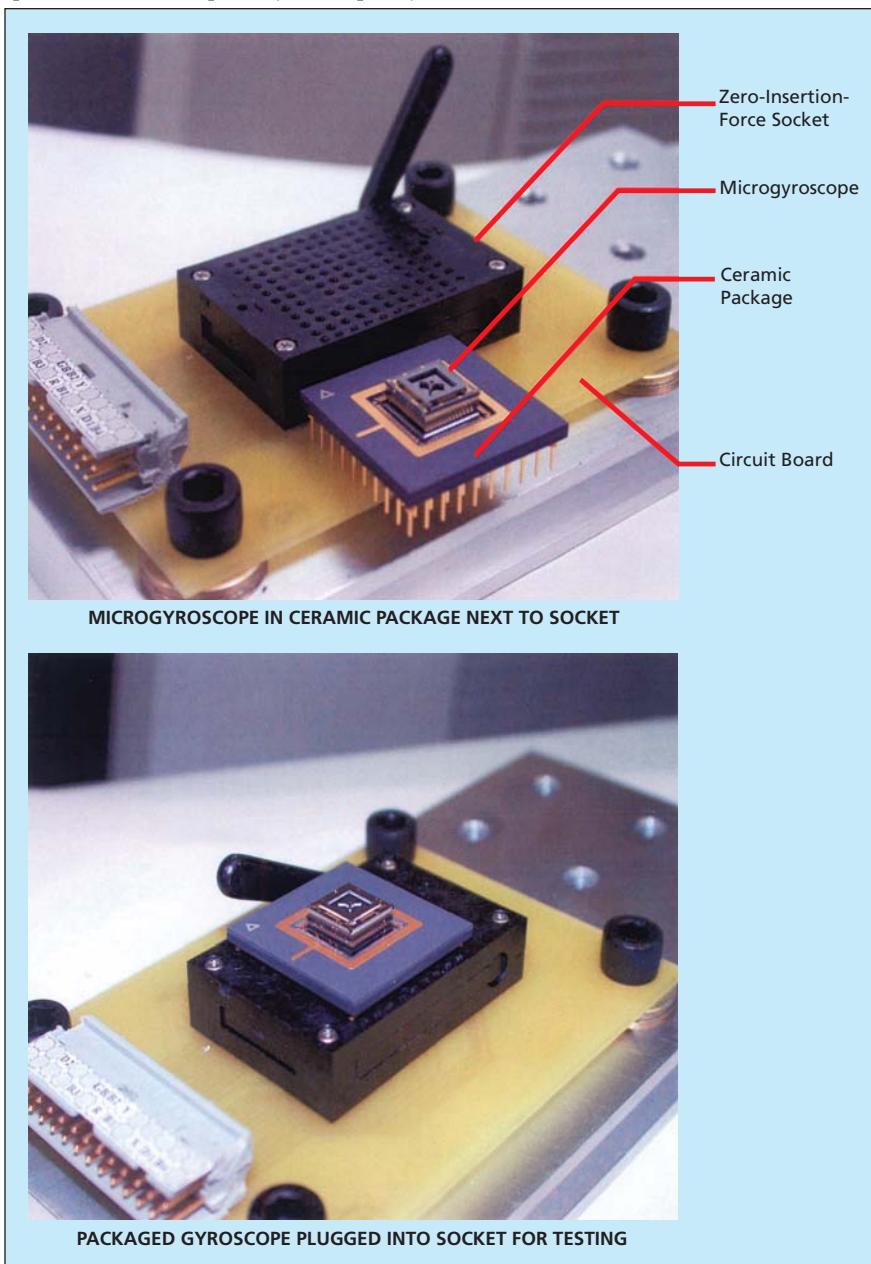
A discussion of pertinent aspects of the unmodified design and the unmodified fabrication process is prerequisite to a meaningful description of the modifications. The design of the microgyroscope package was not conducive to high yield and rapid testing of many microgyroscopes. One of the major impediments to high yield and testing was found to lie in vibration-isolation beams around the four edges of each microgyroscope, which beams were found to be unnecessary for achieving high resonance quality factors ( $Q$  values) characterizing the vibrations of petallike cantilevers.

The fabrication process included an 8- $\mu\text{m}$ -deep plasma etch. The purpose of the etch was to create 8- $\mu\text{m}$  vertical gaps, below which were to be placed large gold evaporated electrodes and sensing pads to drive and sense resonant vibrations of the "petals." The process also included a step in which bridges between dies were cut to separate the dies.

The etched areas must be kept clean and smooth (free of debris and spikes), because any object close to 8  $\mu\text{m}$  high in those areas would stop the vibrations. However, it was found that after the etch, there remained some spikes with heights that were, variously, almost as high or as high as the etch depth. It also was found that the cutting of bridges created silicon debris, some of which lodged in the 8- $\mu\text{m}$  gaps and some of which landed on top of the petals. The masses added to the petals by the debris altered resonance frequencies and/or  $Q$  values to unacceptable degrees. Hence, the spikes and the debris have been conjectured to cause most of the observed malfunctions of newly fabricated microgyroscopes.

Another pertinent aspect of the unmodified design and process was the fabrication of electrodes and the 8- $\mu\text{m}$  capacitance gap on a 500- $\mu\text{m}$ -thick wafer, and the fabrication of a 3-mm-thick baseplate from another wafer. It was necessary to bond these wafers to each other in an assembly step that was later found to be superfluous in that it could be eliminated by a suitable modification of the design.

The modifications include a redesign



A Plug-and-Test Design enables the testing of many microgyroscopes in a short time.

of the microgyroscope package to eliminate the vibration-isolation beams while providing acceptably high  $Q$  values ( $\approx 4 \times 10^4$ ). The modified design includes a plug-in feature for quick testing (see figure). The plasma etch has been replaced by a wet etch, using a specially formulated KOH-based solution, that does not leave spikes. The design of the bridges has been modified to incorporate double notches, such that they can be cut without producing much debris, and a special suction tool resembling one used by a dentist has been developed to collect flying debris during cutting.

The superfluous assembly step has been eliminated by modifying the de-

sign so that all the functional parts previously fabricated on the 500- $\mu\text{m}$  and 3-mm wafers are now fabricated entirely on 3-mm baseplate wafers only. In a previous approach to elimination of the superfluous step, KOH etches were made through 3-mm wafers, then metal patterns were formed by evaporating metals while using shadow masks (not standard practice). In the modified process, the metals are evaporated first (standard practice), then holes are ground by use of a diamond-tipped drill on an index table.

*This work was done by Sam Y. Bae, Karl Y. Yee, and Dean Wiberg of Caltech for NASA's Jet Propulsion Laboratory. Fur-*

*ther information is contained in a TSP (see page 1).*

*In accordance with Public Law 96-517, the contractor has elected to retain title to this invention. Inquiries concerning rights for its commercial use should be addressed to:*

*Innovative Technology Assets Management  
JPL*

*Mail Stop 202-233  
4800 Oak Grove Drive  
Pasadena, CA 91109-8099  
(818) 354-2240*

*E-mail: [iaoffice@jpl.nasa.gov](mailto:iaoffice@jpl.nasa.gov)*

*Refer to NPO-30341, volume and number of this NASA Tech Briefs issue, and the page number.*



## Chamber for Growing and Observing Fungi

Lyndon B. Johnson Space Center, Houston, Texas

A chamber has been designed to enable growth and observation of microcolonies of fungi in isolation from the external environment. Unlike prior fungus-growing apparatuses, this chamber makes it possible to examine a fungus culture without disrupting it. Partly resembling a small picture frame, the chamber includes a metal plate having a rectangular through-the-thickness opening with recesses for a top and a bottom cover glass, an inlet for air,

and an inlet for water. The bottom cover glass is put in place and held there by clips, then a block of nutrient medium and a moisture pad are placed in the opening. The block is inoculated, then the top cover glass is put in place and held there by clips. Once growth is evident, the chamber can be sealed with tape. Little (if any) water evaporates past the edges of the cover glasses, and, hence there is little (if any) need to add water. A microscope can

be used to observe the culture through either cover glass. Because the culture is sealed in the chamber, it is safe to examine the culture without risking contamination. The chamber can be sterilized and reused.

*This work was done by Duane L. Pierson of Johnson Space Center and Thomas C. Molina of KRUG Life Sciences. For further information, contact the Johnson Innovative Partnerships Office at (281) 483-3809. MSC-22904*

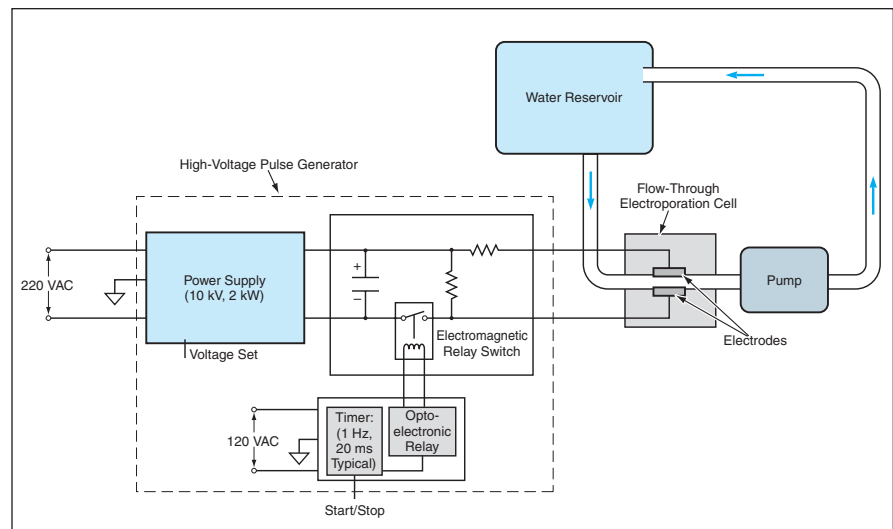
## Electroporation System for Sterilizing Water

Amounts of chemicals needed for sterilization are reduced.

Lyndon B. Johnson Space Center, Houston, Texas

A prototype of an electroporation system for sterilizing wastewater or drinking water has been developed. In electroporation, applied electric fields cause transient and/or permanent changes in the porosities of living cells. Electroporation at lower field strengths can be exploited to increase the efficiency of chemical disinfection (as in chlorination). Electroporation at higher field strengths is capable of inactivating and even killing bacteria and other pathogens, without use of chemicals. Hence, electroporation is at least a partial alternative to chlorination.

The transient changes that occur in micro-organisms at lower electric-field strengths include significantly increased uptake of ions and molecules. Such increased uptake makes it possible to achieve disinfection at lower doses of chemicals (e.g., chlorine or ozone) than would otherwise be needed. Lower doses translate to lower costs and reduced concentrations of such carcinogenic chemical byproducts as trichloromethane. Higher electric fields cause cell membranes to lose semipermeability and thereby become unable to function as selective osmotic barriers between the cells and the environment. This loss of function is the cause of the cell death at higher electric-field intensities. Experimental evidence does not indicate cell lysis but, rather, combined leaking of cell proteins out of the cells as



**High-Voltage Pulses Are Applied** to a pair of electrodes as water flows between them. Depending on the pulse amplitude, the resulting electric field between the electrodes either makes pathogens in the water more vulnerable to a disinfecting chemical or else inactivates them even in the absence of such a chemical.

well as invasion of foreign chemical compounds into the cells.

The concept of electroporation is not new: it has been applied in molecular biology and genetic engineering for decades. However, the laboratory-scale electroporators used heretofore have been built around small (400-microliter) cuvettes, partly because the smallness facilitates the generation of electric fields of sufficient magnitude to cause electroporation. Moreover, most laboratory-scale electroporators have been de-

signed for testing static water. In contrast, the treatment cell in the present system is much larger and features a flow-through geometry, such that electric fields strong enough to effect 99.9-percent disinfection can be applied to water flowing in a pipe.

The figure schematically depicts one version of the prototype system, wherein the output of a high-voltage pulse generator is applied to two electrodes on opposite sides of a flow-through electroporation cell. The pulse amplitude, duration,

and repetition period are chosen to obtain the desired degree of disinfection. Most critical is the amplitude, which is chosen in consideration of the interelectrode gap (1 cm in the prototype) to obtain the needed electric-field intensity. The threshold electric-field intensity for transient changes in permeability and reduced-dosage infection is about 0.2 kV/cm; the threshold for inactivation is about 5 kV/cm. In a practical system, the electroporation cell would be equipped with multiple pairs of electrodes along the flow path and the high-voltage pulses ap-

plied to the pairs would be synchronized so that any given small volume of water would be subjected to multiple high-voltage pulses on its way through the electroporation cell.

Electroporation sterilization technology is best employed in small point-of-entry (POE) and point-of-use (POU) applications as in homes or other small facilities. In smaller pipe diameters, it can be very cost effective, but the power usage becomes excessive in larger water or wastewater treatment facilities. Bioelectromagnetics, however, has developed an alternative

electromagnetic field technology that is very cost effective in large water/wastewater treatment installations.

*This work was done by Kenneth J. Schlager of Bioelectromagnetics, Inc. for Johnson Space*

**Center.** For further information, contact

*Kenneth J. Schlager, President*

*Bioelectromagnetics, Inc.*

*12825 Elmwood Road*

*Elm Grove, WI 53122*

*Phone: (262) 782-2048*

*Fax: (262) 786-1491*

*E-mail: Kjschlag@Execpc.com*

*Refer to MSC-23377.*



## Thermoelectric Air/Soil Energy-Harvesting Device

Small amounts of power would be extracted from natural temperature differences.

NASA's Jet Propulsion Laboratory, Pasadena, California

A proposed thermoelectric device would exploit natural temperature differences between air and soil to harvest small amounts of electric energy. Because the air/soil temperature difference fluctuates between nighttime and daytime, it is almost never zero, and so there is almost always some energy available for harvesting. Unlike photovoltaic cells, the proposed device could operate in the absence of sunlight. Unlike a Stirling engine, which could be designed to extract energy from the air/soil temperature difference, the proposed device would contain no moving parts. The main attractive feature of the proposed device would be high reliability. In a typical application, this device would be used for low-power charging of a battery that would, in turn, supply high power at brief, infrequent intervals for operating an instrumentation package containing sensors and communication circuits.

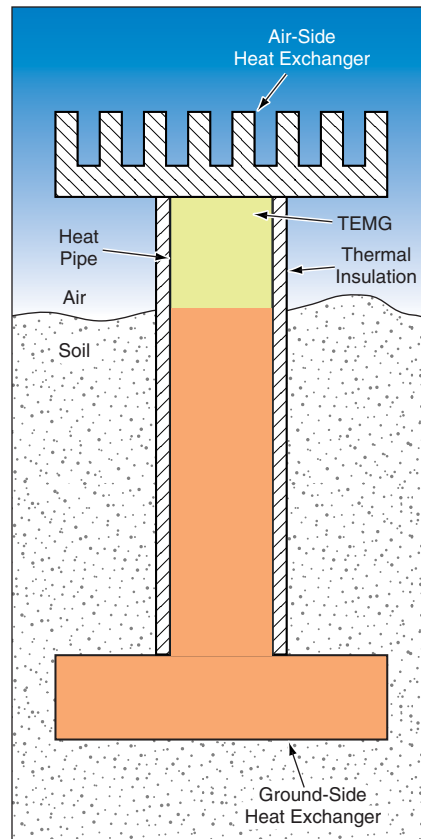
The device (see figure) would include a heat exchanger buried in soil and connected to a heat pipe extending up to a short distance above the ground surface. A thermoelectric microgenerator (TEMG) would be mounted on top of the heat pipe. The TEMG could be of an advanced type, now under development, that could maintain high (relative to prior thermoelectric generators) power densities at small temperature differentials. A heat exchanger exposed to the air would be mounted on top of the

TEMG. It would not matter whether the air was warmer than the soil or the soil warmer than the air: as long as there was a nonzero temperature difference, heat

would flow through the device and electricity would be generated.

A study of factors that could affect the design and operation of the device has been performed. These factors include the thermal conductances of the soil, the components of the device, the contacts between the components of the device, and the interfaces between the heat exchangers and their environments. The study included experiments that were performed on a model of the device to demonstrate feasibility. Because a TEMG suitable for this device was not available, a brass dummy component having a known thermal conductance of 1.68 W/K was substituted for the TEMG in the models to enable measurement of heat flows. The model included a water-based heat pipe 30 in. (76.2 cm) long and 1 in. (2.54 cm) in diameter, wrapped with polyethylene insulation to reduce radial heat flow. Several different side heat exchangers were tested. On the basis of the measurements, it was predicted that if a prototype of the device were equipped with a TEMG, daily temperature fluctuations would cause its output power to fluctuate between 0 and about 0.1 mW, peaking to 0.35 mW during early afternoon.

*This work was done by Jeffrey Snyder, Jean-Pierre Fleurial, and Eric Lawrence of Caltech for NASA's Jet Propulsion Laboratory. Further information is contained in a TSP (see page 1). NPO-30831*



This Simple, Reliable Thermoelectric Device would harvest electric energy from the difference in temperature between air and soil.

## Flexible Metal-Fabric Radiators

Lyndon B. Johnson Space Center, Houston, Texas

Flexible metal-fabric radiators have been considered as alternative means of dissipating excess heat from spacecraft and space suits. The radiators also may be useful in such special terrestrial applications as rejecting heat from space-suit-like protective suits worn in hot work environments. In addition to flexibility and consequent ease of deployment and installation on objects of

varying sizes and shapes, the main advantages of these radiators over conventional rigid radiators are that they weigh less and occupy less volume for a given amount of cooling capacity. A radiator of this type includes conventional stainless-steel tubes carrying a coolant fluid. The main radiating component consists of a fabric of interwoven aluminum-foil strips bonded to

the tubes by use of a proprietary process. The strip/tube bonds are strong and highly thermally conductive. Coolant is fed to and from the tubes via flexible stainless-steel manifolds designed to accommodate flexing of, and minimize bending forces on, the fabric. The manifolds are sized to minimize pressure drops and distribute the flow of coolant evenly to all the

tubes. The tubes and manifolds are configured in two independent flow loops for operational flexibility and protective redundancy.

This work was done by Cynthia Cross and Hai D. Nguyen of **Johnson Space Center**, and Warren Ruenemele, Kambiz K. Andish, and Sean McCalley of Lockheed Martin

Corp. For further information, contact the Johnson Innovative Partnerships Office at (281) 483-3809. MSC-23331

## Actuated Hybrid Mirror Telescope

A new type of lightweight, wide-aperture, precise telescope is under development.

NASA's Jet Propulsion Laboratory, Pasadena, California

The figure depicts the planned Actuated Hybrid Mirror Telescope (AHMT), which is intended to demonstrate a new approach to the design and construction of wide-aperture spaceborne telescopes for astronomy and Earth science. This technology is also appropriate for Earth-based telescopes.

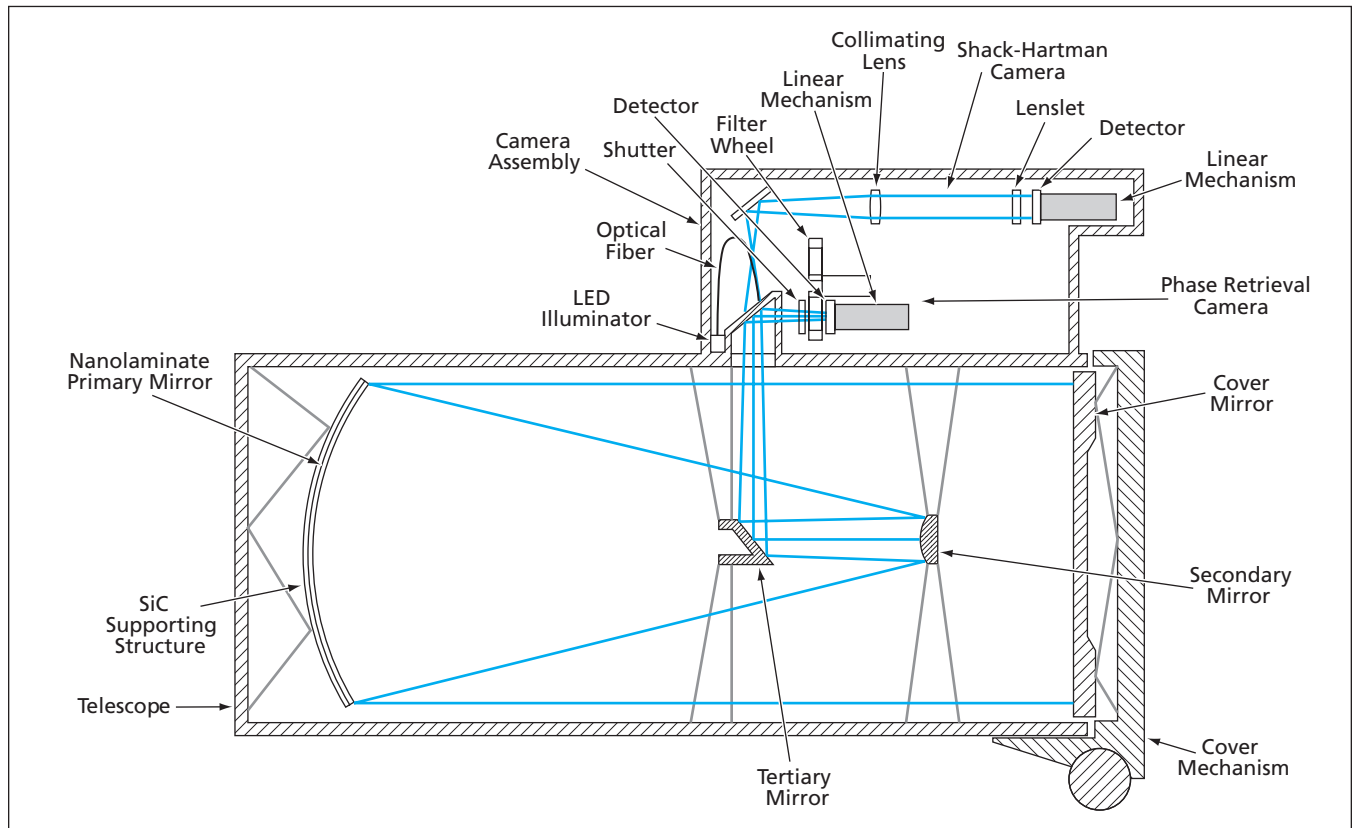
The new approach can be broadly summarized as using advanced lightweight mirrors that can be manufactured rapidly at relatively low cost. More specifically, it is planned to use precise replicated metallic nanolaminate mirrors to obtain the required high-quality optical finishes. Lightweight, dimensionally stable silicon carbide (SiC) structures will support the nanolaminate mirrors in the required surface figures. To enable dif-

fraction-limited telescope performance, errors in surface figures will be corrected by use of mirror-shape-control actuators that will be energized, as needed, by a wave-front-sensing and control system.

The concepts of nanolaminate materials and mirrors made from nanolaminate materials were discussed in several previous *NASA Tech Briefs* articles. Nanolaminates constitute a relatively new class of materials that can approach theoretical limits of stiffness and strength. Nanolaminate mirrors are synthesized by magnetron sputter deposition of metallic alloys and/or compounds on optically precise master surfaces to obtain optical-quality reflector surfaces backed by thin shell structures. As an integral part of the deposi-

tion process, a layer of gold that will constitute the reflective surface layer is deposited first, eliminating the need for a subsequent and separate reflective-coating process. The crystallographic textures of the nanolaminate will be controlled to optimize the performance of the mirror. The entire deposition process for making a nanolaminate mirror takes less than 100 hours, regardless of the mirror diameter.

Each nanolaminate mirror will be bonded to its lightweight SiC supporting structure. The lightweight nanolaminate mirrors and SiC supporting structures will be fabricated from reusable master molds. The mirror-shape-control actuators will be low-power, high-capacitance lead magnesium niobate elec-



The Design of the AHMT will utilize advanced materials and advanced sensing and control techniques to obtain imaging. The primary mirror will have a diameter of 0.75 m and an areal density less than 10 kg/m<sup>2</sup>.

trostrictive actuators that will be embedded in the SiC structures. The mode of operation of these actuators will be such that once power was applied, they will change in length and once power was removed, they will maintain dimensional stability to nanometer precision. This mode of operation will enable the use of low-power, minimally complex electronic control circuitry.

The wave-front-sensing and control system will be designed and built accord-

ing to a two-stage architecture. The first stage will be implemented by a Shack-Hartmann (SH) sensor subsystem, which will provide a large capture range. The second, higher-performance stage will be implemented by an image-based wave-front-sensing subsystem that will include a phase-retrieval camera (PRC), and will utilize phase retrieval and other techniques to measure wavefront error directly. Phase retrieval is a process in which multiple images of an unresolved

object are iterated to estimate the phase of the optical system that acquired the images. The combination of SH and phase-retrieval sensors will afford the virtues of both a dynamic range of  $10^5$  and an accuracy of  $<10$  nm.

*This work was done by Gregory Hickey, David Redding, Andrew Lowman, David Cohen, and Catherine Ohara of Caltech for NASA's Jet Propulsion Laboratory. Further information is contained in a TSP (see page 1). NPO-40105*

## Optical Design of an Optical Communications Terminal

**This airborne system would keep itself aimed at a ground station.**

*NASA's Jet Propulsion Laboratory, Pasadena, California*

An optical communications terminal (OCT) is being developed to enable transmission of data at a rate as high as 2.5 Gb/s, from an aircraft or spacecraft to a ground station. In addition to transmitting high data rates, OCT will also be capable of bidirectional communications. The OCT is meant to incorporate all of the design features of a prior apparatus denoted the Optical Communications Demonstrator (OCD), plus some improvements.

Like the OCD, the OCT would utilize a single telescope aperture for both transmitting and receiving. Also as in the OCD, a fine-steering mirror (FSM) would be included in the transmitting optical train.

The OCT design utilizes a 1,550-nm fiber-optic amplifier transmitter like that

used in the telecommunications industry. Such an amplifier includes a single-mode oscillator, to which one can apply modulation such that the laser light emanating from the fiber can convey data at a rate in the gigabit-per-second range. The laser beam from each such amplifier would be coupled, via a collimating interface module, to a transceiver optical assembly, major optical components of which are shown in the figure.

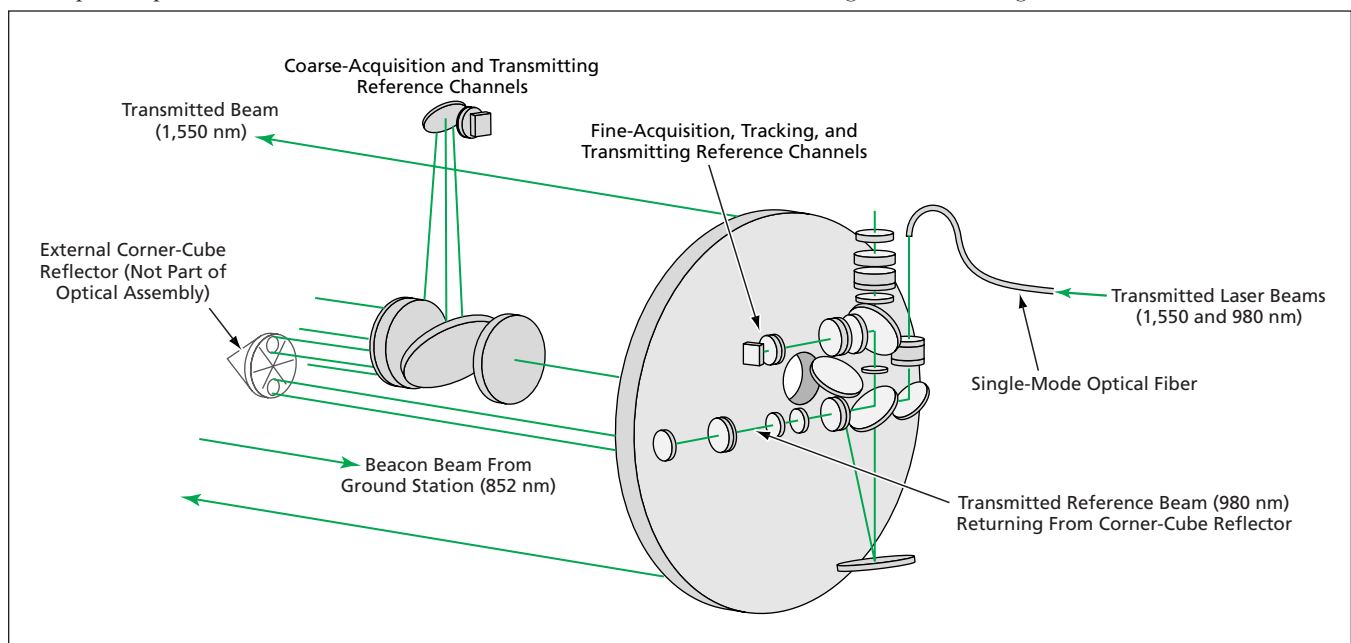
The OCT shall include large-field-of-view focal planes for receiving optical communications and for sensing remote beacon lasers for controlled acquisition, tracking, and pointing (in other words, beacons toward which the OCT would be aimed for transmitting or receiving). The OCT could be connected to a gim-

bal assembly that could be used for coarse aiming.

The OCT would utilize six optical channels — three for transmitting, three for receiving. The transmitting channels would be the following:

- A channel for a 1,550-nm-wavelength laser beam, which would be the main data-modulated beam to be transmitted via the telescope;
- A channel for part of a split 980-nm laser beam used as a reference beam for fine-pointing servo control; and
- A channel for the other part of the split 980-nm beam used for calibration of a coarse-acquisition charge-coupled device (CCD).

The receiving channels would be the following:



The **Optical Assembly of the OCT** would be compact, yet would accommodate six optical channels, each playing a different role in transmission or reception.

- A channel for a portion of an 852-nm-wavelength beacon-and-data-communication signal from a ground station for use in the coarse-acquisition control system;
- A channel for another portion of the 852-nm signal for use in the fine-acquisition-and-tracking system; and
- A channel for yet another portion of the 852-nm signal, used for reception of data from the ground station.

The telescope in the OCT would have an aperture 100 mm wide and would be afocal: all beams would be collimated at the points where they would be split. The design would minimize vignetting and would include field stops, Lyot stops, and baffles to block stray light. To make the optical system compact, the primary mirror would have a focal-length/diameter ratio ("f" number) of 1.2.

In the first-mentioned transmitting channel, the 1,550-nm laser light coming from a single-mode optical fiber would be collimated and directed to a spot on the FSM coincident with a pupil image plane, then reflected from the FSM to a dichroic beam splitter (DBS), then reflected by four more mirrors, the last two of which would be the secondary and primary telescope mirrors. The divergence of the outgoing 1,550-nm laser beam could be tailored by altering the design of the collimating interface module: one would choose the amount of divergence according to

range of the free-space optical link and the degree of mechanical stability of the aircraft to carry the OCT. The FSM could steer the 1,550-nm laser beam over an angular range about 10 milliradians wide.

In the second-mentioned transmitting channel (the one used for reference for fine pointing), the 980-nm laser beam would be made to propagate with the 1,550-nm beam through the single-mode optical fiber and the rest of the optical train until the two beams reach the DBS. At the DBS, a significant fraction of the 980-nm beam would be transmitted through relay optics to a retroreflector. The retroreflected 980-nm beam would be guided back to a second beam splitter, where the reflected fraction would be brought to focus at a focal plane (the fine-acquisition focal plane), the field of view of which would be 10 milliradians wide. Thus, steering by the FSM would change the location of the 980-nm-wavelength beam spot on this focal plane.

The fraction of the 980-nm beam transmitted through the DBS would propagate through the rest of the optical train and out of the telescope along with the 1,550-nm beam. If the telescope were to be deliberately mechanically aimed at an external corner-cube reflector, the reflected portion of the 980-nm would travel back into the telescope, through the DBS, and onto the fine-ac-

quisition focal plane to a spot different from the reference spot mentioned in the previous paragraph.

Another portion of the returning 980-nm beam, constituting the beam in the third-mentioned transmitting channel, would impinge on the coarse-acquisition focal plane (that is, on the coarse-acquisition CCD). This arrangement would facilitate the calibration of co-boresightedness between the coarse-acquisition and fine-steering fields of view.

In the first-mentioned receiving channel, a portion of the 852-nm signal from the ground station would impinge on the coarse-acquisition focal plane, which would have a field of view 3° wide — wide enough to facilitate acquisition under most circumstances. In the second-mentioned receiving channel, a portion of the 852-nm signal would be guided to a focus on the fine-acquisition focal plane. The design would ensure that location of this focus would differ from that of the 980-nm beam. In the third-mentioned receiving channel, the beam splitter would divert a fraction of the received 852-nm beam to a detector that would extract any data signal conveyed as modulation of this beam.

*This work was done by Abhijit Biswas, Norman Page, and Hamid Hemmati of Caltech for NASA's Jet Propulsion Laboratory. Further information is contained in a TSP (see page 1).  
NPO-30537*



## Algorithm for Identifying Erroneous Rain-Gauge Readings

What was previously a subjective manual analysis is automated and made objective.

Marshall Space Flight Center, Alabama

An algorithm analyzes rain-gauge data to identify statistical outliers that could be deemed to be erroneous readings. Heretofore, analyses of this type have been performed in burdensome manual procedures that have involved subjective judgements. Sometimes, the analyses have included computational assistance for detecting values falling outside of arbitrary limits. The analyses have been performed without statistically valid knowledge of the spatial and temporal variations of precipitation within rain events. In contrast, the present algorithm makes it possible to automate such an analysis, makes the analysis objective, takes account of the spatial distribution of rain gauges in conjunction with the statistical nature of spatial variations in rainfall readings, and minimizes the use of arbitrary criteria.

The algorithm implements an iterative process that involves nonparametric statistics. The steps of the algorithm are the following:

1. Raw rain-gauge data are subjected to qualitative tests of validity. The details of the tests are attuned to the details of the sources of data and data-entry procedures. For example, reports that include negative rain-gauge readings or incorrect dates are rejected. Data that pass these tests are accepted for processing in the next step.
2. Associated with each gauge is a neighborhood, defined as that gauge plus the five nearest gauges that (a)

have reported, (b) are currently accepted, and (c) are more than 100 meters distant.

The 100-meter distance criterion is arbitrary, but not totally so: It has been chosen to ensure that each accepted gauge gives a reading independent of that of any other accepted gauge. Independence of readings is basic assumption of the statistical analysis performed in the subsequent steps.

The five-nearest-gauge criterion is also only partly arbitrary: It has been chosen as a compromise between (a) undesired sensitivity to numerical artifacts at fewer gauges per neighborhood and (b) undesired insensitivity to input errors (which the errors that one seeks to detect) at greater numbers of gauges per neighborhood.

3. The six readings from each neighborhood are ranked. If the reading of the gauge under consideration is a local minimum or maximum, then it is deemed erroneous if it is less than one-third or greater than three times the reading of the gauge of the adjacent rank.
4. After rejection of the gauges that have been thus deemed to give erroneous readings, a new set of neighborhoods is computed from the remaining accepted gauges, again following the logic of step 2.
5. The readings from gauges in the new neighborhoods are examined

for errors, again following the logic of step 3.

6. The neighborhood of any gauge in step 3 or step 5 is examined to determine which, if any, other gauges in the neighborhood also were flagged as giving erroneous readings. If all of the gauges in the neighborhood have been flagged and if, in addition, their errors have all been found to be of the same sense (that is, all high or all low), then the readings from the neighborhood are assumed to be correct. The justification for this decision is that it is unlikely that two or more independent, spatially adjacent observations would both be extreme highs or extreme lows. In addition, when a gauge is flagged because of a low reading and the readings of at least three other gauges are zero but are not local minima, then that gauge is not flagged.

The algorithm has been implemented as a series of subroutines in a computer program used to edit sets of rainfall data. The algorithm could also be implemented as a program in its own right or incorporated into other programs for the purpose of identifying erroneous input data pertaining to phenomena other than rainfall.

*This work was done by Doug Rickman of Marshall Space Flight Center. Further information is contained in a TSP (see page 1).  
MFS-31993-1*

## Condition Assessment and End-of-Life Prediction System for Electric Machines and Their Loads

System generates on-line, real-time condition assessment and end-of-life prediction.

Lyndon B. Johnson Space Center, Houston, Texas

An end-of-life prediction system developed for electric machines and their loads could be used in integrated vehicle health monitoring at NASA and in other government agencies. This system will provide on-line, real-time condition assessment and end-of-life prediction of

electric machines (e.g., motors, generators) and/or their loads of mechanically coupled machinery (e.g., pumps, fans, compressors, turbines, conveyor belts, magnetic levitation trains, and others). In long-duration space flight, the ability to predict the lifetime of machinery

could spell the difference between mission success or failure. Therefore, the system described here may be of inestimable value to the U.S. space program.

No known system (hardware, software, or hybrids) currently exists that

performs this function. While there are several software programs used commercially that address various aspects of the off-line diagnostics analysis of rotating equipment — including motors, generators, turbines, and the like — the ineffectiveness of these programs in diagnosing incipient failures is well-documented. Indeed, industry feedback suggests that the majority of these software tools will provide accurate diagnoses in only about 60 to 65 percent of analyzed cases.

The system differs greatly from commercial software because the system will provide continuous monitoring for on-line condition assessment and end-of-life prediction as opposed to the current off-line diagnoses. Similarly, the system will also provide real-time condition assessment and end-of-life prediction as contrasted with the delayed diagnosis of commercially available

software. Indeed, this system also will provide automated condition assessment and end-of-life prediction (not manual fault diagnosis analysis), integrated condition assessment and end-of-life prediction capability (not the current sensor-dependent fault diagnosis analysis), and machine- and/or load-independent condition assessment and end-of-life prediction, which differs significantly from the machine-dependent diagnosis of commercial software systems. In sum, therefore, this invention provides the following new and critical features:

- an all-in-one on-line, real-time condition assessment and end-of-life prediction system for electric machines and their loads;
- a machine- and load-independent condition assessment and end-of-life prediction system; and
- enhanced effectiveness resulting from

the information-processing technologies used.

The system clearly advances the state-of-the-art. Its software is independent of any specific hardware platform, no third-party programs are required for operations, and the system can be implemented with any high- or low-level programming language. Potential users of this software will run the gamut from the space program (for which it was developed) to anyone who maintains electric machines and their loads.

*This work was done by Alexander G. Parlos and Hamid A. Toliyat of Texas A&M University, Departments of Mechanical and Electrical Engineering for **Johnson Space Center**. For further information, contact:*

*Alexander G. Parlos*

*E-mail: a-parlos@tamu.edu*

*Refer to MSC-22894, volume and number of this NASA Tech Briefs issue, and the page number.*



### **Lightweight Thermal Insulation for a Liquid-Oxygen Tank**

A proposed lightweight, reusable thermal-insulation blanket has been designed for application to a tank containing liquid oxygen, in place of a non-reusable spray-on insulating foam. The blanket would be of the multilayer-insulation (MLI) type and equipped with a pressure-regulated nitrogen purge system. The blanket would contain 16 layers in two 8-layer sub-blankets. Double-aluminized polyimide 0.3 mil ( $\approx 0.008$  mm) thick was selected as a reflective shield material because of its compatibility with oxygen and its ability to withstand ionizing radiation and high temperature. The inner and outer sub-blanket layers, 1 mil ( $\approx 0.025$  mm) and 3 mils ( $\approx 0.076$  mm) thick, respectively, would be made of the double-aluminized polyimide reinforced with aramid. The inner and outer layers would provide structural support for the more fragile layers between them and would bear the insulation-to-tank attachment loads. The layers would be spaced apart by lightweight, low-thermal-conductance netting made from polyethylene terephthalate.

*This work was done by G. Scott Willen, Jennifer Lock, and Steve Nieczkoski of Technology Applications, Inc. for Johnson Space Center. For further information, contact:*

*Technology Applications, Inc.  
5445 Conestoga Court, #2A  
Boulder, CO 80301-2724  
Telephone No.: (303) 443-2262  
www.techapps.com.  
Refer to MSC-23099.*

### **Stellar Gyroscope for Determining Attitude of a Spacecraft**

A paper introduces the concept of a stellar gyroscope, currently at an early stage of development, for determining the attitude or spin axis, and spin rate of a spacecraft. Like star trackers, which are commercially available, a stellar gyroscope would capture and process images of stars to determine the orientation of a spacecraft in celestial coordinates. Star trackers utilize charge-coupled devices as image detectors and are capable of tracking attitudes at spin rates of no more than a few degrees per second and update rates typically  $< 5$  Hz. In contrast, a stellar gyroscope would utilize an active-pixel sensor as an image detector and would be capable of tracking attitude at a slew rate as high as  $50^\circ/\text{s}$ , with an update rate as high as 200 Hz. Moreover, a stellar gyroscope would be capable of measuring a slew rate up to  $420^\circ/\text{s}$ . Whereas a Sun sensor and a three-axis mechanical gyroscope are typically needed to complement a star tracker, a stellar gyroscope would function without them; consequently, the mass, power consumption, and mechanical complexity of an attitude-determination system could be reduced considerably.

*This work was done by Bedabrata Pain, Bruce Hancock, Carl Liebe, and Jeffrey Mellstrom of Caltech for NASA's Jet Propulsion Laboratory. Further information is contained in a TSP (see page 1).  
NPO-30481*

### **Lifting Mechanism for the Mars Explorer Rover**

A report discusses the design of a rover lift mechanism (RLM) — a major subsystem of each of the Mars Exploration Rover vehicles, which were landed on Mars in January 2004. The RLM had to satisfy requirements to (1) be foldable as part of an extremely dense packing arrangement and (2) be capable of unfolding itself in a complex, multistep process for disengaging the rover from its restraints in the lander, lifting the main body of the rover off its landing platform, and placing the rover wheels on the platform in preparation for driving the rover off the platform. There was also an overriding requirement to minimize the overall mass of the rover and lander. To satisfy the combination of these and other requirements, it was necessary to formulate an extremely complex design that integrated components and functions of the RLM with those of a rocker-bogie suspension system, the aspects of which have been described in several prior *NASA Tech Briefs* articles. In this design, suspension components also serve as parts of a 4-bar linkage in the RLM.

*This work was done by Joseph Melko, Theodore Iskenderian, Brian Harrington, and Christopher Voorhees of Caltech for NASA's Jet Propulsion Laboratory. Further information is contained in a TSP (see page 1).  
NPO-40875*







National Aeronautics and  
Space Administration